REPORT ONR-CR212-259-1F

LEVEL II

ANALYSIS OF T-2C HIGH ANGLE OF ATTACK FLIGHT TEST DATA WITH NONLINEAR SYSTEM IDENTIFICATION METHODOLOGY

JAMES H. VINCENT
W. EARL HALL, JR.
JEFF G. BOHN

SYSTEMS CONTROL, INC. (VT)
1801 PAGE MILL ROAD
PALO ALTO
CALIFORNIA
94304

CONTRACT No. N00014-72-C-0328

FINAL REPORT
Approved for public release; distribution unlimited.

PREPARED FOR THE
OFFICE OF NAVAL RESEARCH • 800 N. QUINCY ST. • ARLINGTON, VA. 22217

UNCLASSIFIED

SECURITY CLASSIFICATION OF THIS PAGE (When Data Entered)

REPORT DOCUMENTATION PAGE	READ INSTRUCTIONS BEFORE COMPLETING FORM
1. REPORT NUMBER: ONR CR212-259-1F	2. GOVT ACCESSION NO.: AD-A086 327
3. RECIPIENT'S CATALOG NUMBER	
4. TITLE (and Subtitle): ANALYSIS OF T-2C HIGH ANGLE OF ATTACK FLIGHT TEST DATA WITH NONLINEAR SYSTEM IDENTIFICATION METHODOLOGY.	5. TYPE OF REPORT & PERIOD COVERED: FINAL REPORT. 3 APR 1972 — 31 MAY 1978
6. PERFORMING ORG. REPORT NUMBER	
7. AUTHOR(s): James H. Vincent, W. Earl Hall, Jr., Jeff G. Bohn	8. CONTRACT OR GRANT NUMBER(s): N0014-72-C-0328
9. PERFORMING ORGANIZATION NAME AND ADDRESS: SYSTEMS CONTROL, INC. (Vt), 1801 Page Mill Road, Palo Alto, CA 94304	10. PROGRAM ELEMENT, PROJECT, TASK AREA & WORK UNIT NUMBERS: 61153N, RR0140101, 5410
11. CONTROLLING OFFICE NAME AND ADDRESS: OFFICE OF NAVAL RESEARCH, 800 N. Quincy Street, Arlington, Virginia 22217	12. REPORT DATE: MAR 1980
	13. NUMBER OF PAGES: 88 (139)
14. MONITORING AGENCY NAME & ADDRESS(if different from Controlling Office)	15. SECURITY CLASS. (of this report): UNCLASSIFIED
	15a. DECLASSIFICATION/DOWNGRADING SCHEDULE

16. DISTRIBUTION STATEMENT (of this Report)

Approved for public release; distribution unlimited.

17. DISTRIBUTION STATEMENT (of the abstract entered in Block 20, if different from Report)

18. SUPPLEMENTARY NOTES

19. KEY WORDS (Continue on reverse side if necessary and identify by block number)

system identification
parameter identification
nonlinear aerodynamic modeling
T-2C flight test
flying qualities

20. ABSTRACT (Continue on reverse side if necessary and identify by block number)

This study represents one of the first thorough applications of advanced nonlinear system identification techniques to the problem of determining aircraft aerodynamic characteristics in the maximum-lift flight regime, and has produced results confirming the ability of these methods to develop realistic and useful dynamics models for flight test data and to provide a valuable guide for data acquisition system specification in future flight test programs. This

DD FORM 1 JAN 73 1473 EDITION OF 1 NOV 65 IS OBSOLETE

UNCLASSIFIED

SECURITY CLASSIFICATION OF THIS PAGE (When Data Entered)

389333

20. ABSTRACT (Continued)

study also demonstrated the value of employing wind tunnel data and theoretical (or empirical) aerodynamic analyses during the model structure determination stage in order to begin with a basic familiarity with the nature of nonlinearities to be encountered.

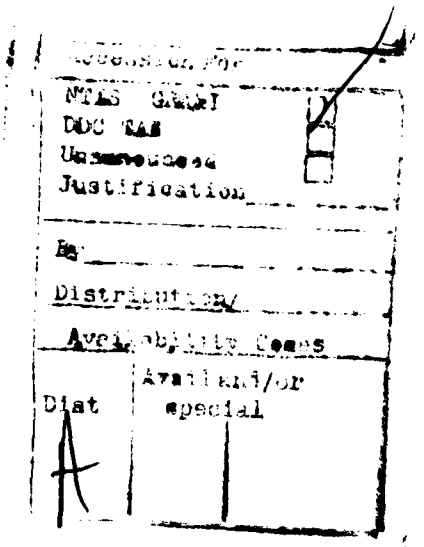

TABLE OF CONTENTS

I. INTRODUCTION AND SUMMARY

1.1 INTRODUCTION

The need for improved modeling of aircraft aerodynamic characteristics has been, and continues to be, apparent in numerous areas of great operational importance. Reliable and accurate flight simulators for pilot training, verification of design methods for specification of aircraft characteristics, and the off-line development of mission profiles that make optimum use of the airplane's capabilities (without exceeding its limitations) are three such areas. In general, there is also a need for improved <u>understanding</u> of an airplane's intrinsic aerodynamic characteristics which, if filled, will lead to improved cost effectiveness and operational safety.

The ability to process large quantities of data from flight tests has led to the parallel development of data processing algorithms which greatly increase the amount of useful knowledge that can be extracted from the data. These algorithms based on dynamical and statistical principles, yield very precise information about the characteristics of the data and the system that produced it.

1.2 BACKGROUND

The present study represents the application of an advanced system identification methodology which has been developed specifically for estimating high-angle-of-attack aerodynamics stability and control coefficients from flight data. The development of this methodology has been documented extensively in previous technical reports and technical journals, and is summarized historically as follows.

the algorithms on linear aircraft response data. This was done in a two-step process by processing F-14 data from the Naval Air Test Center and subsequently installing the software at NATC. The identification program installed at NATC had the ability to identify both process and measurement noise and the operation of these programs is detailed in Ref. 5. The program was further applied to other aircraft by NATC personnel as discussed in Refs. 6 and 7.

(4) Application of the software to simulated and actual flight test data indicated the need for a near real-time identification algorithm to provide rapid estimates of aircraft linear stability and control derivatives. A theoretical basis for such reduced computation time was established with further research, resulting in two complementary algorithms. The first algorithm was based on the theory of Luenberger canonical forms for linear systems and reduced execution time of the linear maximum likelinood algorithm by a factor of ten (depending on the number of parameters to be identified). The second algorithm was based on a new formulation of an instrumental-variables approach [8] and provided true real-time estimation capability for linear aircraft stability derivatives. The theoretical development and implementation of these two algorithms, with application to simulated and actual flight test data, is presented in Ref. 5.

(5) The developments of the previous phases had demonstrated the further requirements for expansion of the theoretical base upon which nonlinear system identification was based. Specific research into both the nonlinear model structure determination and input design issues was performed, the results of which are reported in Ref. 6.

The results of this report are the application of the identification methodology to actual nonlinear aerodynamic regime data. The data for this analysis were provided by the Naval Air Development Center. The specific objectives are listed in Table 1.1.

TABLE 1.1. OBJECTIVES

• DETERMINE NONLINEAR T-2 AERODYNAMIC COEFFICIENTS AND MODEL STRUCTURES IN HIGH ANGLE OF ATTACK AND SIDESLIP REGIMES.
• EVALUATE MODEL CHARACTERISTICS AGAINST EXISTING DATA.
• EVALUATE MODEL PARAMETERS.
• DEMONSTRATE ADVANCED NONLINEAR IDENTIFICATION TECHNIQUES.

1.3 SUMMARY

Subsequent sections of this report are organized as follows. Section II discusses the T-2C flight data analyzed in this effort, and describes wind tunnel data and theoretical aerodynamic techniques used as a guide in model structure determination. Section III describes the data preparation techniques employed, and the application and findings of the model structure determination and model parameter estimation techniques. Section IV summarizes the study results and presents conclusions and recommendations.

Various detailed technical data are presented in the appendices.

II. T-2C AERODYNAMIC DATA BASE

2.1 OVERVIEW

This section discusses the flight test data used in the determination of T-2C high angle of attack aerodynamic coefficients through model development and parameter estimation, and data used to support modeling efforts and give additional understanding of aircraft characteristics. Wind tunnel data and theoretical aerodynamic calculations were used to validate each other and provide a reference of comparison for the identified models. In this way, as thorough an understanding of T-2C aerodynamics as could be obtained was developed to guide the aerodynamic model analysis.

2.2 FLIGHT TEST DATA

The flight test data analyzed in this study were taken from flights made between 5 November 1975 and 26 August 1976. The aircraft configuration during these flights is summarized in Table 2.1; it represents the normal, clean aircraft configuration. Detailed aircraft geometry from Ref. 9 is given in Appendix A.

The initial condition for all flight maneuvers was nominally as summarized in Table 2.2; small deviations from the desired trim condition were accounted for in the data analysis procedure. Significant to the goal of nonlinear aerodynamic coefficient determination are the high initial value of C_L and the Reynolds number. The trim angle of attack is just 3.5^0 below the stall angle of attack predicted by both wind tunnel data and theoretical methods (to be discussed below), and the trim lift coefficient of $C_{L_{TRIM}} = .93$ is 78 percent of trim $C_{L_{MAX}}$. Because the flight and wind tunnel Reynolds numbers are quite close (7.5×10^6 vs 4×10^6, respectively), any differences between flight and wind

TABLE 2.1. T-2 FLIGHT AIRCRAFT CONFIGURATION SUMMARY

- CLEAN CONFIGURATION
  - FLAPS NEUTRAL (3° UPRIG)
  - AILERONS NEUTRAL (3° UPRIG)
  - GEAR UP
  - SPEED BRAKE RETRACTED
- NEARLY CONSTANT WEIGHT
  - 11,400 LBS $\pm$ 400 LBS
- THROTTLES FIXED DURING MANEUVERS
- INERTIAS (SLUG-FT^2)

  I_x = 9000

  I_y = 14,600

  I_z = 19,000

  I_{xz} = 0.0

TABLE 2.2 FLIGHT TEST CONDITION

V $\approx$ 300 FT/SEC (TAS)

MACH = 0.3

h = 25,000 FT (PRESSURE)

W = 11,400 LB

γ_{TRIM} = 0.0

REYNOLDS NUMBER = 7.5×10^6

$\alpha_{TRIM} \approx 10.5°$

$C_{L_{TRIM}} = .93$

$C_{L_{MAX}} = 1.2$

NOTE: DATCOM ANALYSIS SHOWS NEGLIGIBLE COEFFICIENT VARIATION DUE TO CHANGE FROM WIND TUNNEL $R_N = 4 \times 10^6$ TO FLIGHT $R_N = 7.5 \times 10^6$

tunnel characteristics are most likely due to effects from other than Reynolds number. Theoretical studies, using DATCOM predictions, verify this conclusion.

Large perturbation maneuvers were initiated at this flight condition by various deflections of one or more control surfaces, with the goal of forcing the aircraft into the stall and post stall regions of angle of attack with sizeable sideslip excursions. Seventeen maneuvers, shown in Table 2.3, were selected for analysis in this study. The types of control inputs employed are sketched

TABLE 2.3. T-2C FLIGHT TEST CONDITIONS USED FOR NONLINEAR AERODYNAMIC IDENTIFICATION

DATE	FLT. TEST NO.	INPUT
NOV. 5, 1975	5	δ_e AFT, FULL δ_r
	9	δ_e AFT, FULL δ_a
DEC. 10, 1975	4	δ_e RANDOM
	8	δ_a RANDOM
	14	SEQUENTIAL DOUBLETS
DEC. 29, 1975	2	δ_e DOUBLET
	14	δ_r RANDOM
	17	SEQUENTIAL RANDOM ($\beta_t = 0°$)
AUG. 26, 1976	1	δ_e RAMP + SINE
	2	SEQUENTIAL RANDOM ($\beta_t = -5°$)
	3	SEQUENTIAL RANDOM ($\beta_t = +5°$)
	4	δ_e AFT + PULSES
	5	LIMIT CYCLE
	6	SHALLOW BANK TO STALL
	7	STEEP BANK TO STALL
	8	PULL UP TO STALL
	9	COORDINATED SPIN ENTRY

in Figure 2.1. These inputs were made by the pilot and are therefore neither repeatable nor precise with regard to their spectral characteristics, but are generally effective in creating large-amplitude motions. A useful indication of excitation effectiveness is a raw-data α-β plot (histogram) such as shown in Figure 2.2, which provides knowledge about the type of information that can be obtained from the maneuver. Histograms of other flight maneuvers are shown in Section III. Overall, the maneuvers encompassed angles-of-attack from -4° to +30° and angles-of-sideslip in excess of $\pm$20°.

The apparent effect of stall entry dynamics (i.e., deceleration rate and pitch rate) on $C_{L_{MAX}}$ is not an issue since the identification of C_L (see Section III) is based on accelerometer and airspeed measurements. With this approach the problem of relating C_L to air speed via the weight of the aircraft for non "1g" flight is avoided. In general, because the aerodynamic parameters are identified through the minimization of accelerometer, airdata and rate gyro measurements, it is extremely desirable for the system identification techniques described in this report to maximize the dynamic nature of the flight test maneuver.

Flight data were simultaneously recorded on board and telemetered to a ground receiving station. Flight instrumentation provided 6-DOF measurement capability for both rates and acceleration. The types and locations of the sensors are shown in Table 2.4, and their respective ranges shown in Table 2.5. Note that body-axis angular accelerations are measured by using translational accelerometers at the airplane's nose, tail, and wingtips.

2.3 WIND TUNNEL DATA

An extensive wind tunnel investigation of the high-α characteristics of the T-2C is reported in Ref. 9, presenting estimates of static aerodynamic coefficients and control effectiveness

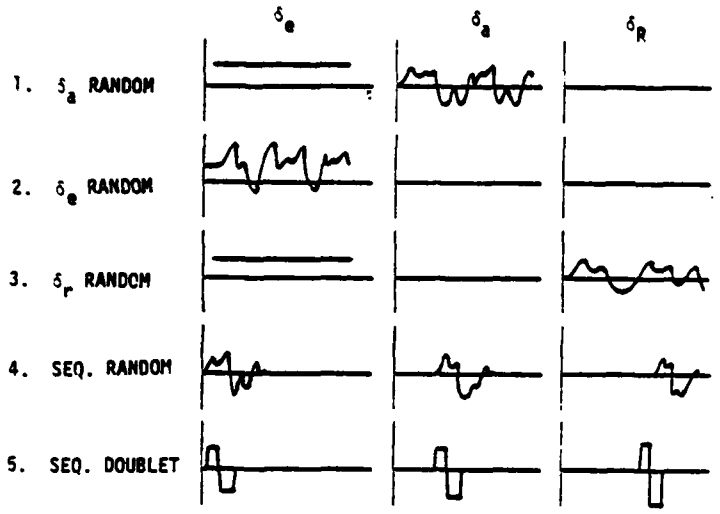

Figure 2.1. Control Inputs for Parameter Identification

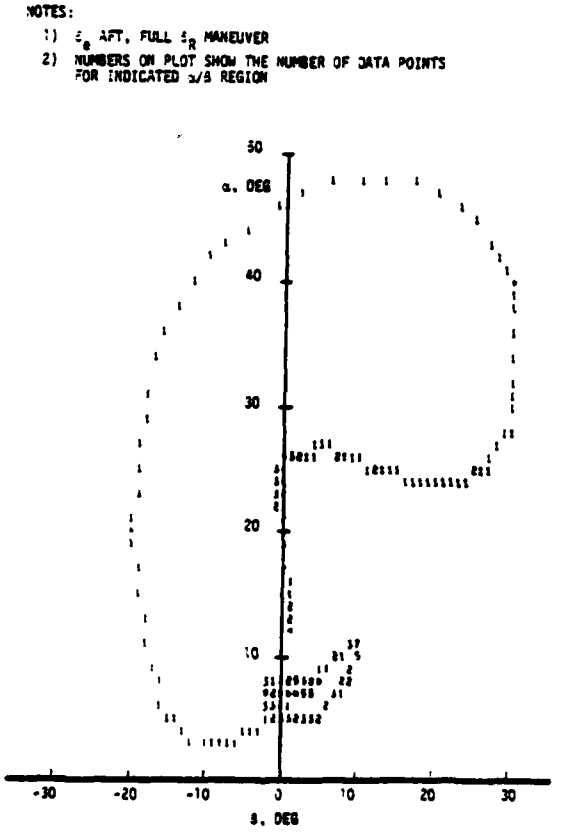

Figure 2.2. Example α/β Histogram

TABLE 2.4. INSTRUMENT LOCATIONS ON YT-2B FOR AIRFRAME DYNAMICS IDENTIFICATION PROGRAM

FUNCTION	NAME	FUSELAGE STATION	WING STATION	WATER LINE
n_x	GREENLEAF SERIAL 1655000-A #674	37.	-4.	-11.
n_z (c.g.)	GIANNINI #1816 24117P-3.5-20	207.	-1.	-21.
n_z NOSE (FOR $\dot{q}$)	GIANNINI #1819 24117P-3.5-20	34.	-6.	-11.
n_z TAIL (FOR $\dot{q}$)	GIANNINI #1837 24117P-3.5-20	366.5	0	+9.
$\dot{q}$	STAHAM ANG. ACC. AA196-8-350	230.	0	-23.5
θ	GIANNINI MODEL SERIAL 5812 3416	56.	0	5.
ϕ	GIANNINI MODEL SERIAL 3812 3416	56.	0	5.
r	NORDEN RG 228 SERIAL #185	47.	0	3.5
p	HUMPHREY G20-1021-00 SERIAL #828	52.	0	2.5
q	NORDEN RG 228 SERIAL #183	196.	0	-22.5
n_y NOSE (FOR $\dot{r}$)	EDELCLIFF MODEL 7-30 SERIAL #366.5	31.5	-6.	-11.
n_y (c.g.)	EDELCLIFF MODEL 7-30 SERIAL #4444	204.	-1.5	-19.
n_z WING TIP (FOR $\dot{p}$)	GIANNINI #1685 24117P-3.5-20	249.	206.5	15.
n_z WING TIP (FOR $\dot{p}$)	GIANNINI #1681 24117P-3.5-20	249.	-206.5	15.
α	VANE	-62.3	0	-21
β	VANE	-65.9	0	-21

NOTE: NEGATIVE WING STATIONS ARE TOWARD LEFT WING. NEGATIVE WATER LINE POSITIONS ARE BELOW FUSELAGE REFERENCE LINE.

TABLE 2.5. MEASUREMENT RANGES FOR YT-2B/C TRANSDUCERS

MEASUREMENT	RANGE
n_z	±3.5g
n_x	±1.0g
n_y	±1.0g
q	±20 DEG/SEC
θ	±15 DEG
r	±20 DEG/SEC
$\dot{q}$	±450 DEG/SEC^2
ϕ	±90 DEG
p	±45 DEG/SEC
v	0 - 500 KTS (COARSE) 0-50 ICTS (FINE RESETTABLE)
α	±10 DEG ABOUT SET POINT
β	±10 DEG

parameters. The overall ranges of simultaneous α and β settings in the reference study were -8° to +83° and -10° to +30°, respectively, accomplished by the use of three different model support arrangements, each allowing examination of a particular range of α within which sting interference with the model was small.

Figures 2.3 and 2.5 (Ref. 9) show basic lift, drag, and pitching moment coefficient data for $\beta = 0$ over the entire α range. Figures 2.6 and 2.7 show the variation of rolling and yawing moment coefficients with sideslip angle at various angles of attack.

These wind tunnel data were very useful in the present investigation. Through study of the nonlinear aerodynamic characteristics revealed in the data, the nonlinear functional forms of the coefficients were obtained with less effort during the model structure determination stage. Knowledge of key performance and stability parameters, such as $C_{L_{MAX}}$, $\alpha_{C_{L_{MAX}}}$, and C_{m_α}, allowed faster interpretation of flight data characteristics and permitted reasonableness checks on the hypothesized functional forms of the coefficients. Any uncertainty in the wind tunnel data did not substantially impair its usefulness in this effort, as it was demonstrated in the work to follow that the MSD and parameter estimation techniques require only basic, qualitative a priori knowledge of aircraft characteristics.

2.4 THEORETICAL AERODYNAMIC DATA

Theoretical methods for computing aircraft aerodynamic characteristics are necessary in order to confirm wind tunnel data and provide estimates of aerodynamic parameters not amenable to experimental determination. It is desirable that the capabilities of theoretical methods be well understood, as they provide an opportunity to reduce the extent of wind tunnel testing required to gain an understanding of basic configuration characteristics.

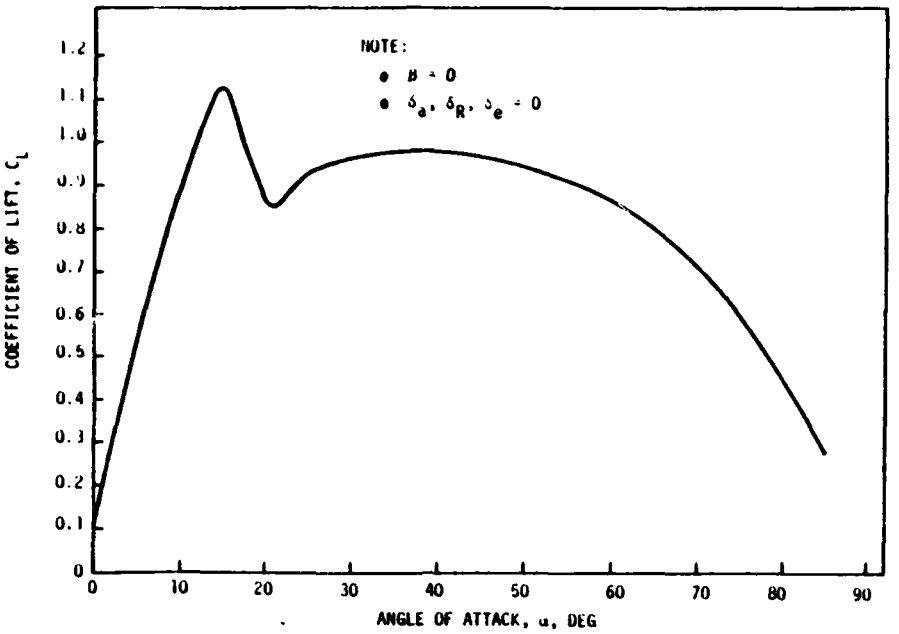

Figure 2.3. T-2C Lift Coefficient Versus Angle of Attack (Wind Tunnel Data from NADC-73259-30)

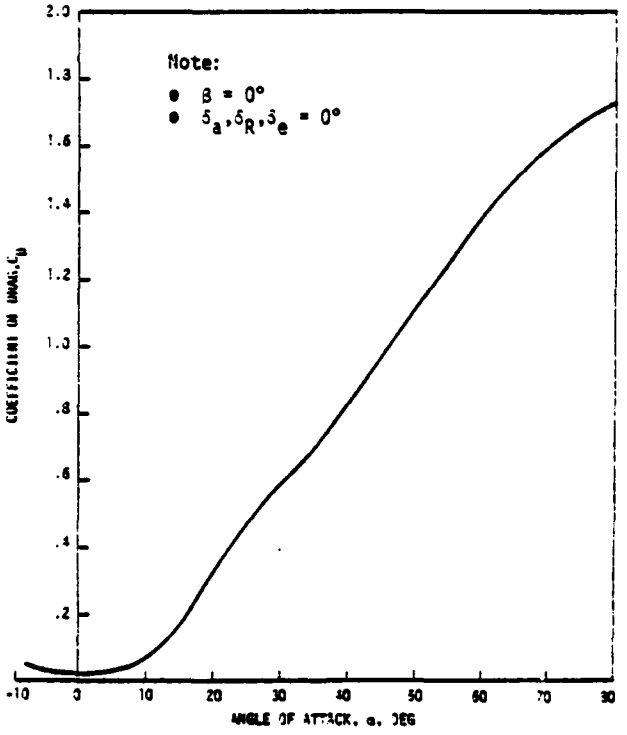

Figure 2.4. T-2C Drag Coefficient Versus Angle of Attack (Wind Tunnel Data from NADC-73259-30)

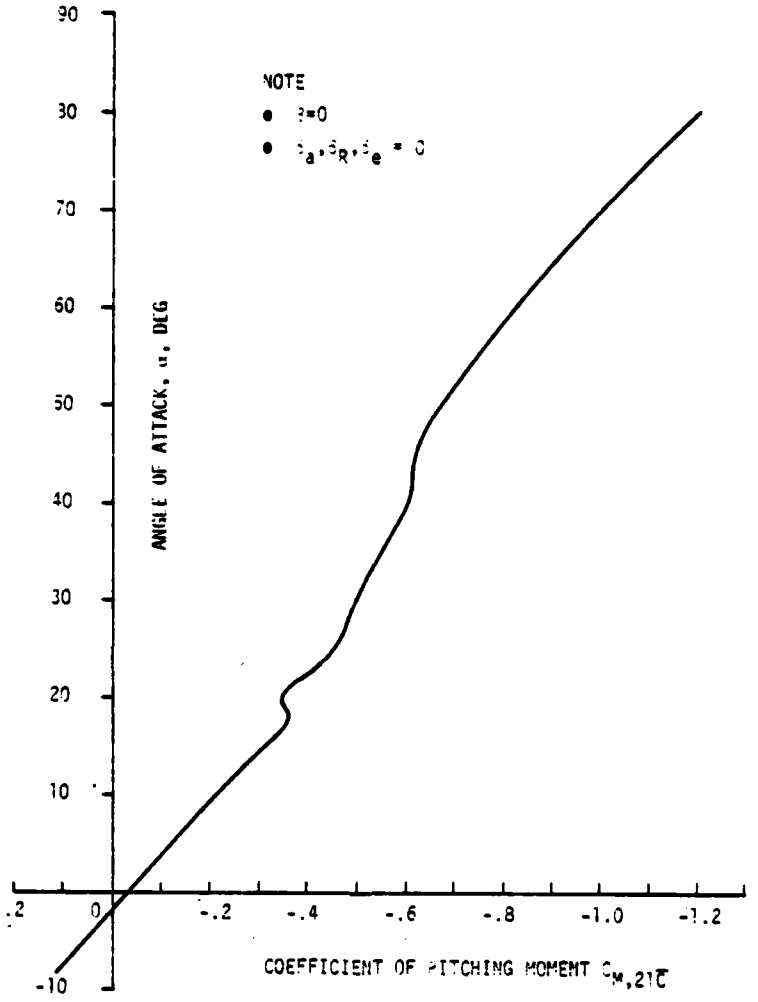

Figure 2.5. T-2C Pitching Moment Coefficient vs. Angle of Attack (Wind Tunnel Data from NADC-73259-30)

NOTE: WIND TUNNEL DATA FROM NADC-73259-30

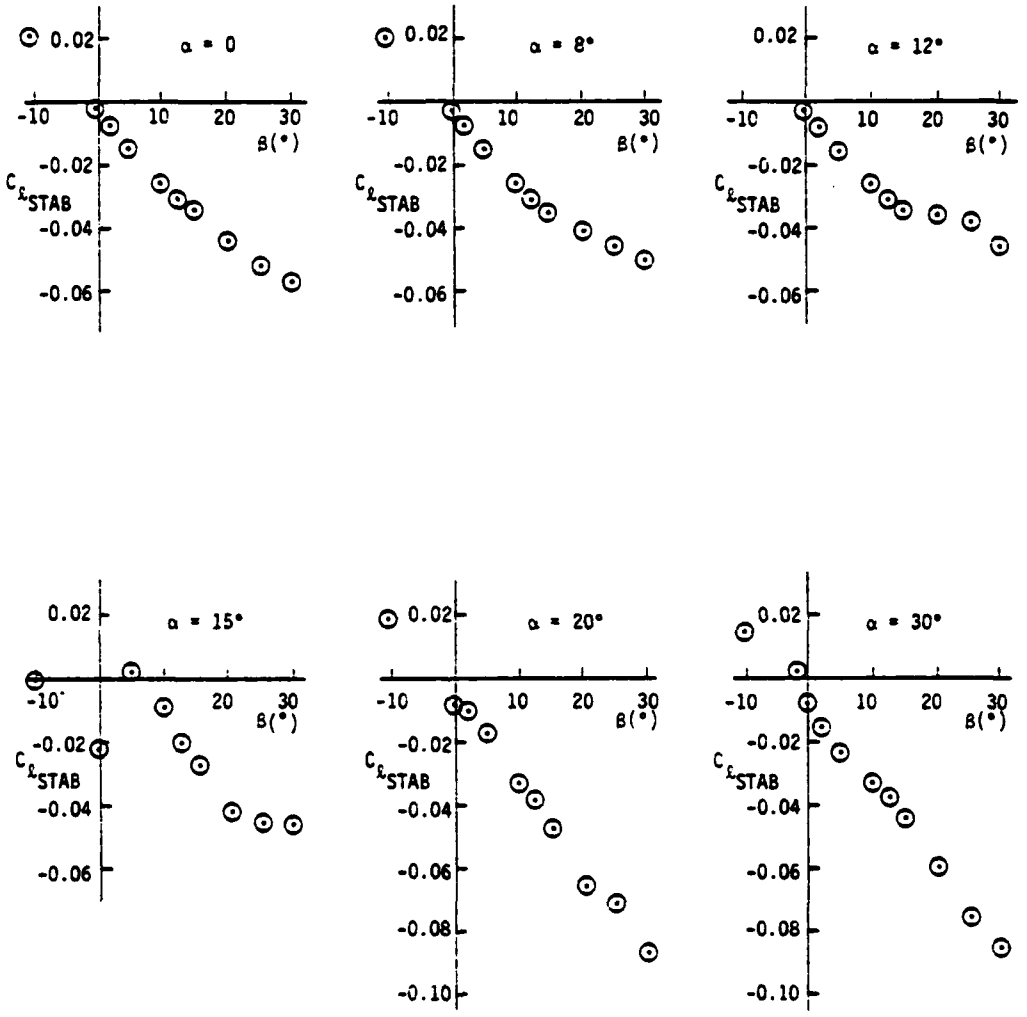

Figure 2.6. T-2C Rolling Moment Coefficient vs. Sideslip (Wind Tunnel from NADC-73259-30)

NOTE: WIND TUNNEL DATA FROM NADC-73259-30

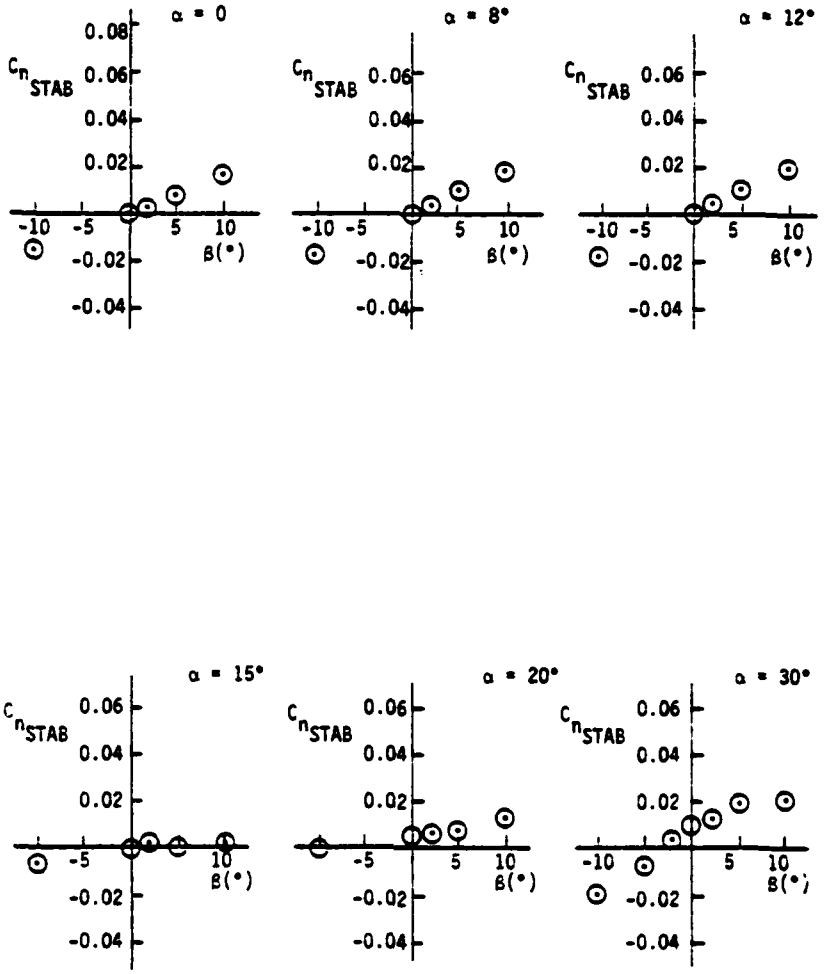

Figure 2.7. T-2C Yawing Moment Coefficients vs. Sideslip (Wind Tunnel Data from NADC-73259-30)

Theoretical aerodynamic methods exist in a wide variety of forms extending from the implementation of closed-form, configuration-dependent equations to elaborate potential flow methods using vortex lattices or source panels to represent the aircraft. The latter approach is typically very complex and costly in terms of computer time, while the former is usually unable to handle the critical matter of downwash distribution and the contributions of horizontal and vertical tail loads. A compromise approach has been reached in the methods of the DATCOM, which is based on wind tunnel data unified by proven theoretical results. This method gives aerodynamic characteristics of a wide range of possible configurations to the accuracy required for preliminary design studies. The utility of the procedure, which is thorough but laborious, has been enhanced manyfold by its incorporation in a digital computer program. The user, by inputting only basic configuration data, may thus easily obtain estimates of static and dynamic aerodynamic coefficients and derivatives, several extending into the nonlinear range of α and β. The burden is on the user, however, to understand the limitations of the methods and recognize those areas in which the predictions may be inaccurate.

One of the key benefits of this method is the ability it brings to examine the effects of small changes from the wind tunnel model configuration. The effects of changing Reynolds number, for instance, or of removing the 3^0 uprig in the T-2C flaps and ailerons, were studied in this effort.

For a relatively simple aircraft configuration such as the T-2C, the DATCOM predictions for basic characteristics possess a high degree of credibility at angles-of-attack below stall. Figure 2.8 shows the lift curve prediction compared to wind tunnel data. Lift curve slope, stall angle of attack, and post-stall lift behavior are all in good agreement with wind tunnel findings. The good prediction of stall α is valuable because of its importance in spline curve fitting for model structure determination. Figure 2.9 shows the pitching moment curve, which displays good agreement with wind tunnel data below stall. Among the other results obtained

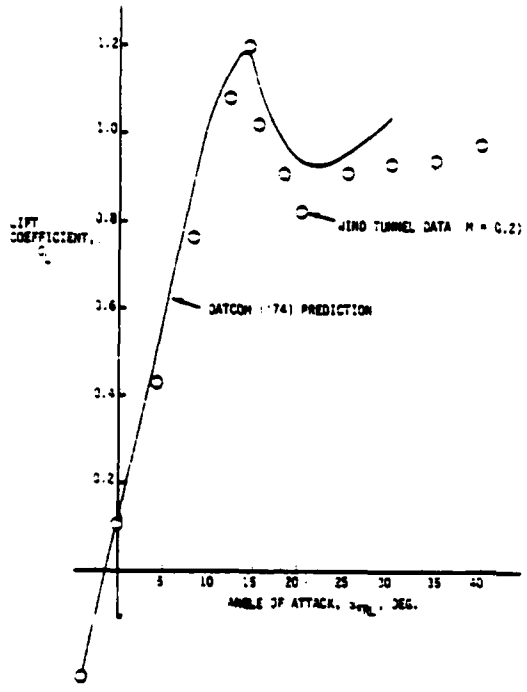

Figure 2.8. T-2C Comparison of Datcom and Wind Tunnel Pitching Moment Prediction

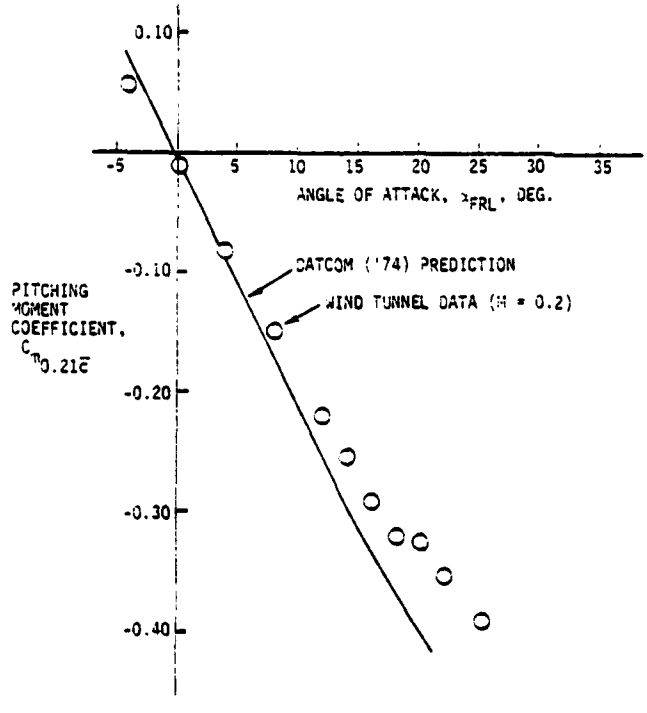

Figure 2.9. T-2C Comparison of Datcom and Wind Tunnel Lift Prediction

are lateral-directional damping and coupling derivatives, of which four important coefficients are shown in Figures 2.10 to 2.13. The DATCOM predictions are compared, in these figures, to theoretical estimates computed by aerodynamic strip theory methods as described in Ref. 10. The general agreement shown here is encouraging.

With the knowledge thus obtained, from wind tunnel and theoretical methods, of aerodynamic parameters of known importance to flight dynamics analysis, the evaluation of flight data is begun to verify or alter these parameters and search for new, non-linear parameters whose determination can result in improved dynamic predictions.

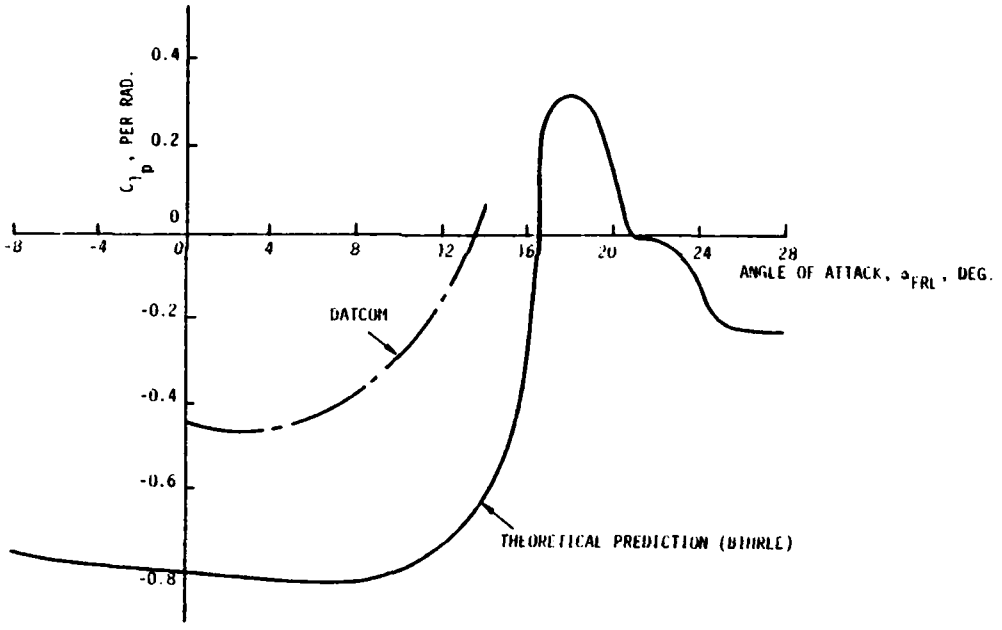

Figure 2.10. Comparison of $C_{\ell p}$ Predictions

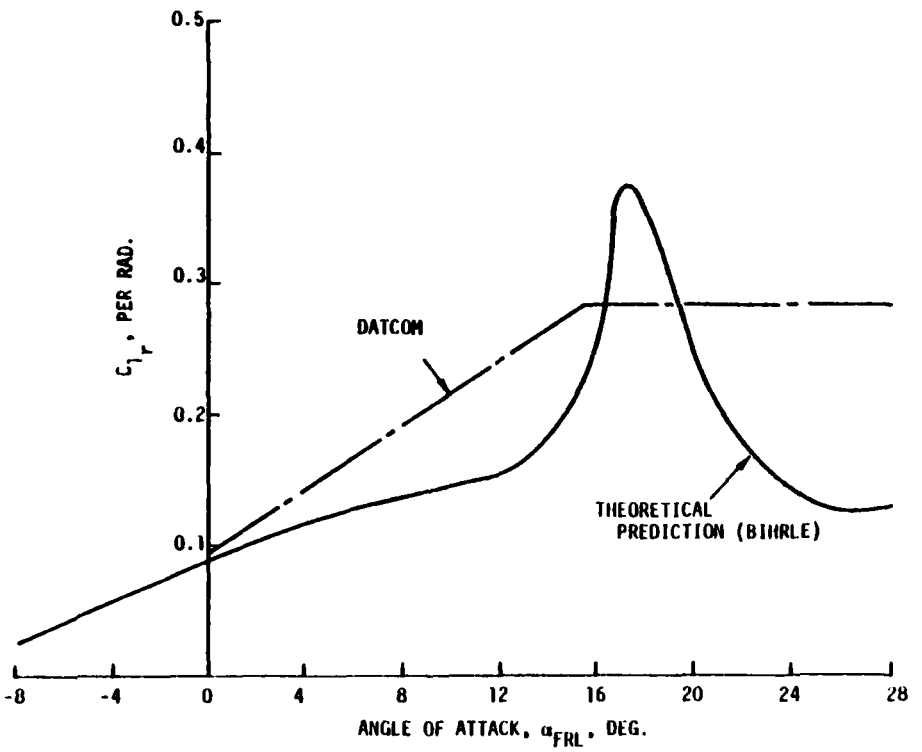

Figure 2.11. Comparison of C_{ℓ_r} Predictions

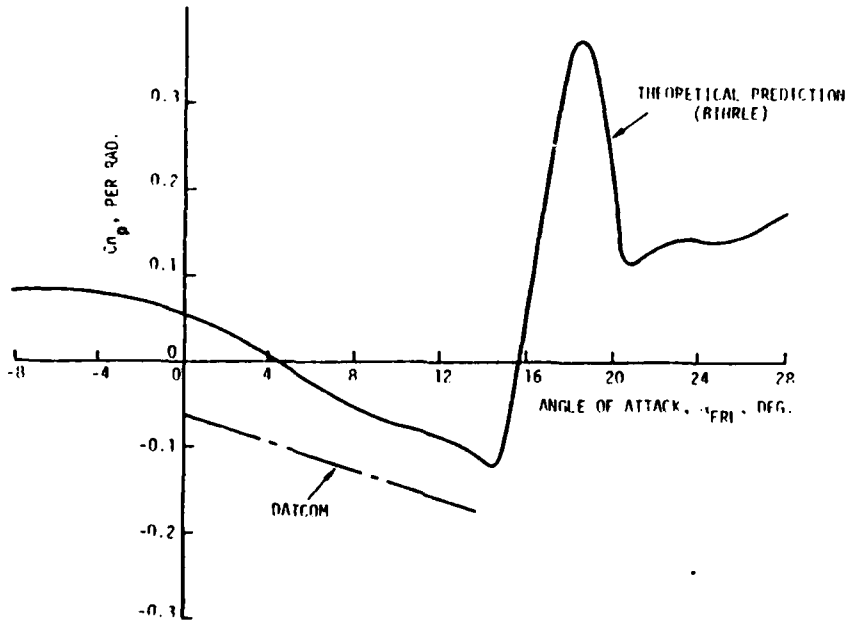

Figure 2.12. Comparison of C_{n_p} Predictions

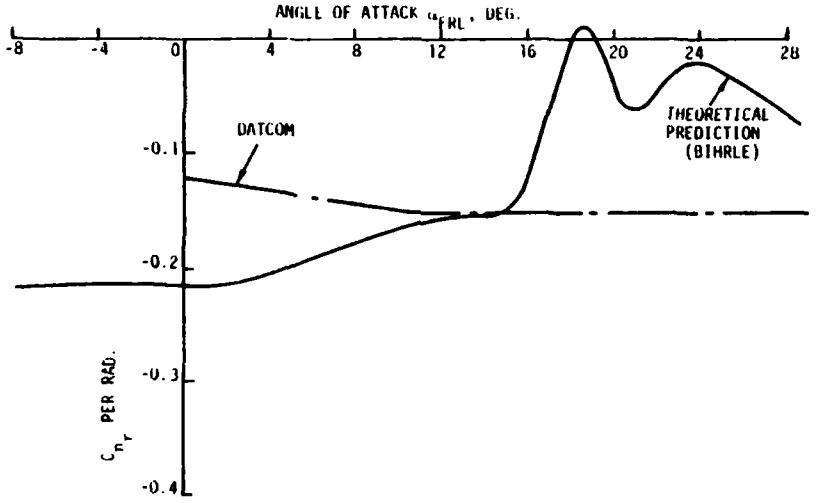

Figure 2.13. Comparison of C_{n_r} Predictions

III. T-2C SYSTEM IDENTIFICATION RESULTS

3.1 OVERVIEW

This section discusses the application of the system identification process to T-2 flight test data and presents the results of the nonlinear aerodynamic modeling analyses. The objective of this effort was to obtain, from flight data, a set of nonlinear functional relationships describing the aerodynamic characteristics of the airplane, in the form of force and moment coefficients and stability derivatives expressed as functions of various combinations of angle of attack and sideslip, rotational rates, and control deflections. Dynamic nonlinear effects such as aerodynamic hysteresis were also sought.

The steps in the integrated system identification procedure for the T-2C are summarized in Figure 3.1 Five basic steps are shown:

(1) Data preparation (reconstruction and filtering).

(2) Model structure determination.

(3) Model parameter estimation.

(4) Model verification.

(5) Flight test planning.

The first four steps comprise the scope of the current contract and are discussed in detail in this chapter. The last step, Flight Test Planning, is reported in Ref. 11.

3.2 FLIGHT DATA PROCESSING

A significant element of the system identification procedure is the preprocessing of the flight test data. The overall objective of this step is to develop a set of kinematically

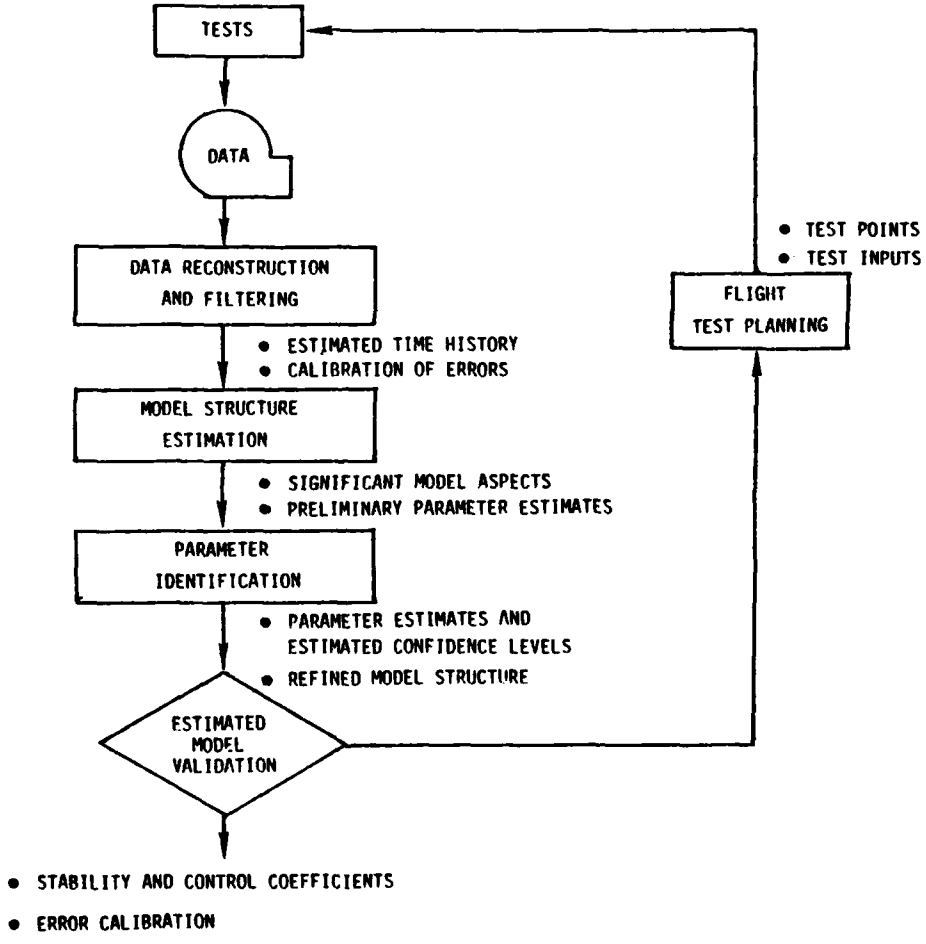

Figure 3.1. Integrated System Identification Procedure

consistent measurements for the model structure determination and parameter identification algorithms. Measurement consistency has a significant impact on parameter identification accuracy since unaccounted for inconsistencies will bias the parameter estimates. The steps followed in the preprocessing of T-2C flight test data are now described.

3.2.1 Data Response Review

The time responses were examined to establish the validity of the SCI-created data files, to classify the flight conditions in terms of aerodynamic regimes which were encountered, and to provide a preliminary assessment of data quality and consistency. From the preliminary assessment, requirements for filtering noisy data were established, wild points and data drop-outs were visually isolated and corrected, and obvious measurement sign errors were identified.

Figure 2.2 illustrates one of the methods used to classify a test condition. This figure is a histogram of angle of attack and sideslip. The numbers in the plot indicate the number of data points within a particular α/β region.

3.2.2. Data Reconstruction

Data reconstruction is an essential subtask of the flight data processing procedure and it comprises three steps.

First, since the equations of motion which are processed by the identification algorithms assume a rigid body formulation, flight measurements representative of the motion at the center of gravity are required. Table 3.1 lists the equations which are used for the reconstruction of equivalent c.g. measurements.

Second, noisy data are filtered to provide numerical conditioning. The T-2C flight test data were processed with a Martin-Graham digital filter. This digital filter has the property

TABLE 3.1. EQUATIONS USED TO RECONSTRUCT C.G. MEASUREMENTS

- VERTICAL & RATE GYROS DO NOT REQUIRE CORRECTION
- AIR DATA SYSTEM
  - * AIRSPEED DOES NOT REQUIRE CORRECTION
  - * $\alpha_{cg} = \text{Tan}^{-1} \left[\text{Tan}\ \alpha_M + \frac{\ell_{x\alpha} Q}{V_T\ \text{Cos}\alpha_M}\ \text{Cos}\beta_M\right]$
  - * $\beta_{cg} = \text{Sin}^{-1} \left[\text{Cos}\ \alpha_M\ \text{Tan}\ \beta_M - \frac{\ell_{x\beta} R}{V_T}\right]$
- ACCELEROMETER

* $a_{x_{cg}} = a_x + (Q^2 + R^2)l_{x_a} + (\dot{R} - PQ)\ell_{y_a} - (PR + \dot{Q})\ell_{z_a}$

* $a_{y_{cg}} = a_y - (PQ + \dot{R})\ell_{x_a} + (P^2 + P^2)\ell_{y_a} + (\dot{P} - RQ)\ell_{z_a}$

* $a_{z_{cg}} = a_z + (\dot{Q} - PR)\ell_{x_a} - (RQ + \dot{P})\ell_{y_a} + (Q^2 + P^2)\ell_{z_a}$

of not changing either the magnitude or phase content of the data up to the cutoff frequency and then truncating the signal for frequencies greater than the termination frequency. For the T-2C application, the cutoff frequency was set at 2Hz and the termination frequency at 4Hz. Since the selected cutoff frequency for the Martin-Graham filter is much greater than the T-2's rigid body frequencies of motion, its application will not change the information content of the flight test data.

The third step involves reconstruction of measurements found (as a result of performing a kinematic consistency evaluation) to be unuseable, and by combining actual measurements to formulate needed values. An example of the first type of reconstruction would be to define roll acceleration by taking the time derivative of roll rate.

Deriving roll acceleration by taking the difference between normal acceleration signals from right and left wing tip accelerometers is an example of the second type of reconstruction. Both types of reconstruction were used for processing the T-2C flight test data.

3.2.3 Data Consistency Analysis

The kinematic consistency of the sensor signals is evaluated as a means of highlighting potential measurement system errors. Measurement system errors can result from a number of possible sources. Bias and scale factor errors could result from using an incorrect calibration curve or from the sensor's power supply not operating at its design condition. Since a body axis frame of reference is used for solving the equations of motion, the orientation of the sensor system relative to the body axis system must be accurately known. Instruments, such as a vertical gyro (VG), can produce erroneous measurements as a result of their operational characteristics. For example, if the VG's erection circuit is allowed to operate during accelerated flight, the attitude measurements will be referenced to a false vertical, and thus will be in error. This type of problem would be most significant for the identification of low frequency modes of motion. Another source of inconsistency exists when inertial velocity components are not measured (this is the case for the T-2C program). Since the equations of motion are written in terms of inertial velocity components, substitution of air referenced components (i.e., $V_T \cos\beta \cos\alpha$ for u) will produce biased answers when winds are present and not accounted for.

An example of a data consistency check is shown in Figure 3.2, where the variation of $\dot{q}$ with time does not agree with dq/dt (q from a rate gyro) or with $\dot{q}$ computed from θ and ϕ from vertical gyro). The latter two approaches agree with each other, so the conclusion is that the $\dot{q}$ measurement is faulty and should be replaced with one of the other (derived) measurements.

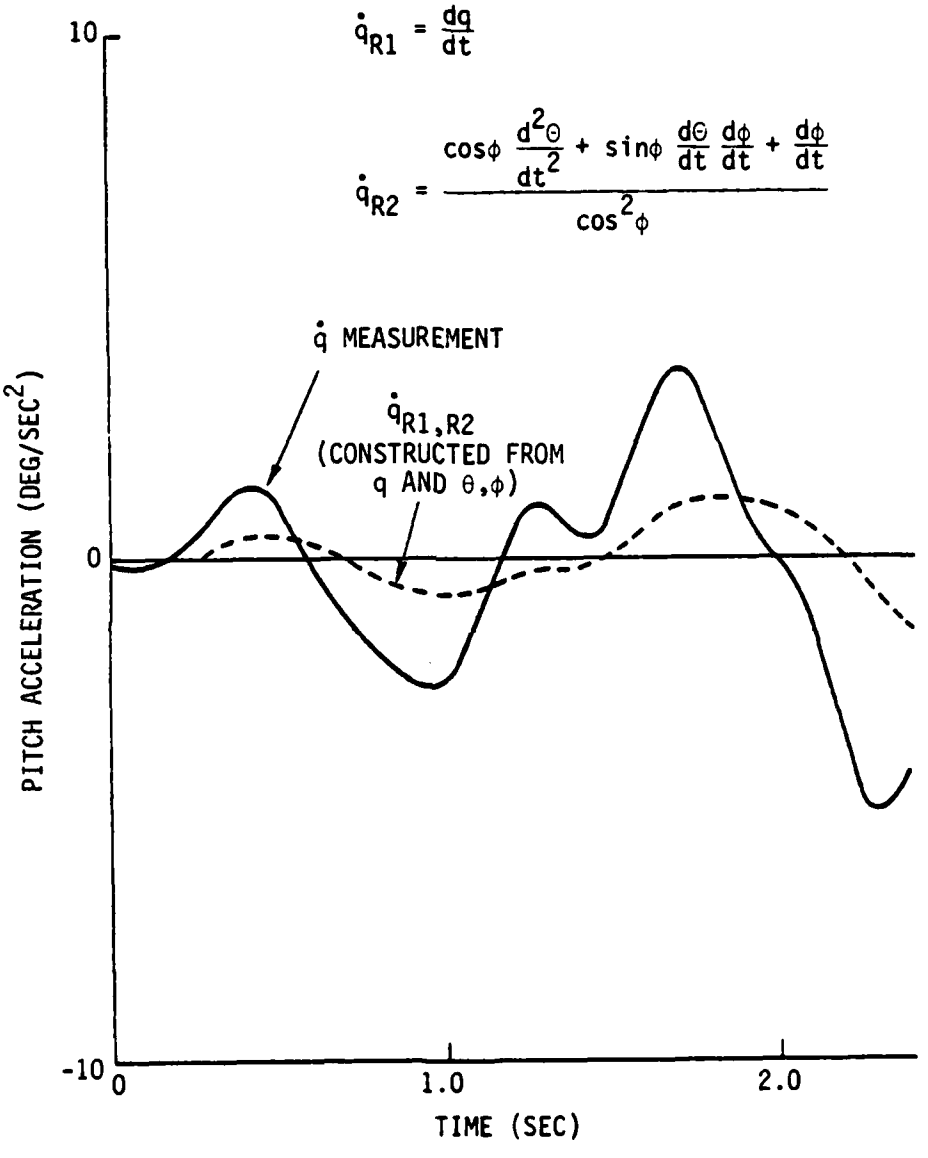

Figure 3.2 Example of Reconstruction and Consistency Checks

3.2.4 T-2C Flight Data Quality

As a result of processing the T-2C flight test data, as described in the preceding sections, the following observations are made about its quality:

(1) The data has a high noise content and requires filtering.

(2) Angular acceleration signals are kinematically inconsistent with body axis rotational velocities and the Euler orientations. Angular acceleration was reconstructed by differentiating the body axis rotational velocities. This reconstruction was performed in the frequency domain with a fast Fourier transformation algorithm.

(3) For some of the flight conditions, the body axis yaw rate signal (r) is inconsistent with the roll rate, lateral acceleration and sideslip measurements. The absence of an airplane heading signal (Ψ) made the identification of correction terms for R difficult.

(4) The angle-of-attack measurement requires both a scale factor and bias correction term to make the side force equation consistent (i.e., $\dot{\beta} = -R + (\tan\alpha)P + A_y/V_T + g\cos\theta\sin\phi/V_T$).

3.3 MODEL STRUCTURE DETERMINATION

System identification is a systematic methodology for analyzing test data to obtain maximally accurate dynamic equation coefficient estimates. Its application to multivariable nonlinear systems, however, requires an additional step before actual identification of parameters is attempted. This step is a mathematical model determination stage where, of all possible nonlinear aerodynamic effects postulated, those of greatest significance are isolated and retained for further analysis. There are two basic reasons for this reduction of order. First, a complete nonlinear model places severe computational demands on parameter identification algorithms; hence, the model generally must be reduced in order. Secondly, if all possible aerodynamic contributions are retained, the problem is "overparameterized" by the inclusion of terms which are not identifiable. This may produce divergence of the identification algorithm. The following subsections

present an overview of the model structure determination procedure, the formulation of the T-2 aerodynamic structure, and the selected model structure.

3.3.1 Overview of Model Structure Determination

The model structure determination procedure is illustrated in Figure 3.3; it includes the following tasks: model structure hypothesis, data processing to define the most significant model parameters, and, finally, model validation.

3.3.1.1. Model Structure Hypothesis

Wind tunnel data, theoretical data and a general understanding of aircraft aerodynamic characteristics comprise the a priori information on which functional models were first based in this effort. While the aerodynamic characteristics of the T-2C contain no significant surprises, such information as the stall angle of attack, the shape of the post-stall lift curve, drag level and polar shape, and the basic nonlinear characteristics of stability and damping derivatives provided useful guidance in the initial formulation of the aerodynamic model structures.

Wind tunnel data, properly reduced and corrected, are the best source of most a priori aerodynamic information. However, the effects of Reynolds number, model support interference, and minor configuration changes are often difficult to account for when correcting the data from wind tunnel to full scale. The best source of dynamic derivative estimates (pitch damping, roll damping, etc.) is theory, since these parameters cannot be accurately determined in a wind tunnel. Theoretical methods are thus a valuable supplement to the experimental data, allowing examination of the sensitivity of the aerodynamic data to configuration and flight condition parameters. To the extent that theoretical methods can supplant wind tunnel testing, their continued development will be useful to model

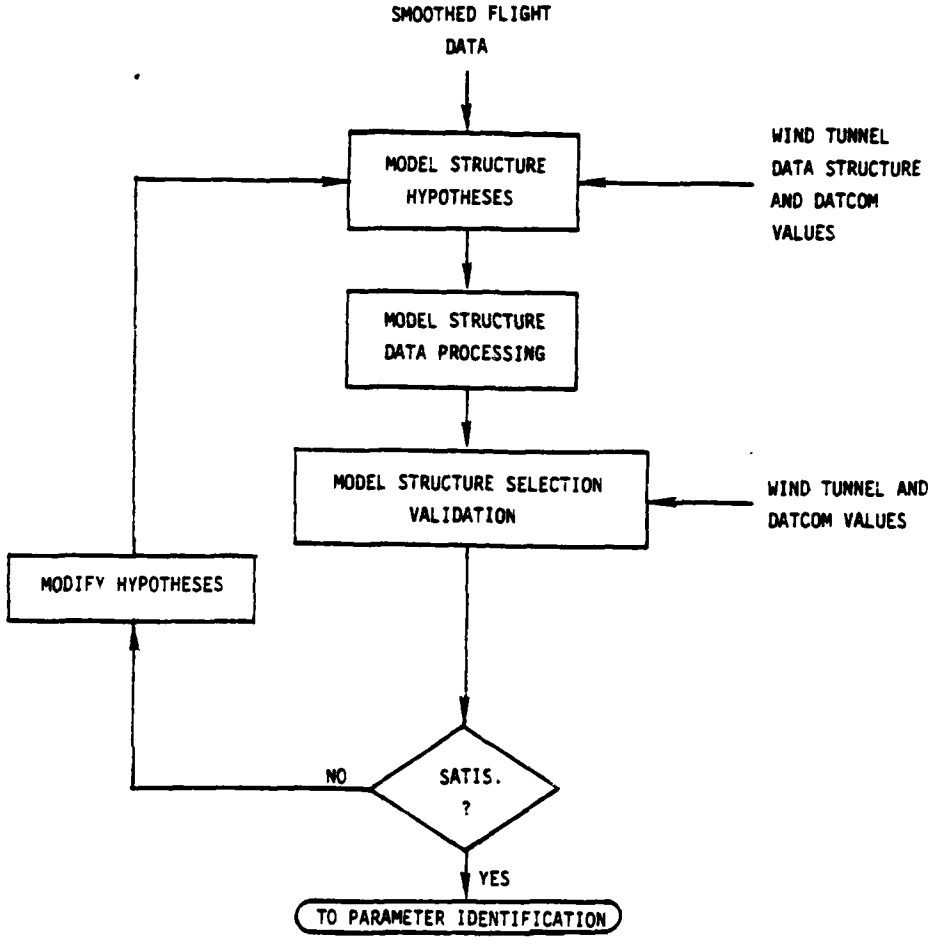

Figure 3.3. Elements of Model Structure Determination

structure determination methods. T-2 theoretical and wind tunnel aerodynamic data were reviewed in Chapter 2.

Model structure hypothesis is the task of using a priori information to formulate functional relationships between the aerodynamic force and moment coefficients and the independent variables (e.g., α, β, P, δ_r, etc.). This process is illustrated by the following example for the yawing moment coefficient equation.

(1) Select the independent variables:

$$C_n = f(\alpha, \beta, P, R, \delta_R, \delta_a)$$

or i.e., yawing moment coefficient is a function of angle-of-attack, sideslip, roll and yaw rate, rudder and aileron position

(2) Partition independent variables into reasonable groups:

$$C_n = \Delta C_{n_{SIDESLIP}} + \Delta C_{n_{DYNAMIC}} + \Delta C_{n_{RUDDER}} + \Delta C_{n_{AILERON}}$$

(3) Select functional relationships for each group:

$$\Delta C_{n_{SIDESLIP}} = (K_{N1} + K_{N2}\alpha + K_{N3}\Delta\alpha_1 + K_{N4}\Delta\alpha_2)\beta + K_{N5}\Delta\beta$$

To effectively handle a nonlinear aerodynamic model, such as that required for the T-2C, a spline model form is adopted. The spline terms (i.e., $\Delta\alpha_1$, $\Delta\alpha_2$, $\Delta\beta$ in the above equation) are piecewise continuous polynomials. The nature of the spline approach is graphically defined in Figure 3.4. Because the spline terms are defined over a restricted region, two modeling benefits result: (1) only lower order terms are required, and (2) prediction error for model extrapolation is low. Spline models have the additional advantage that they can be formulated directly from an understanding of aircraft characteristics as shown in the example (Figure 3.4) and their calculation (or influence) can be controlled by logic

- A PRIORI DATA
  WIND TUNNEL
  CHARACTERISTICS

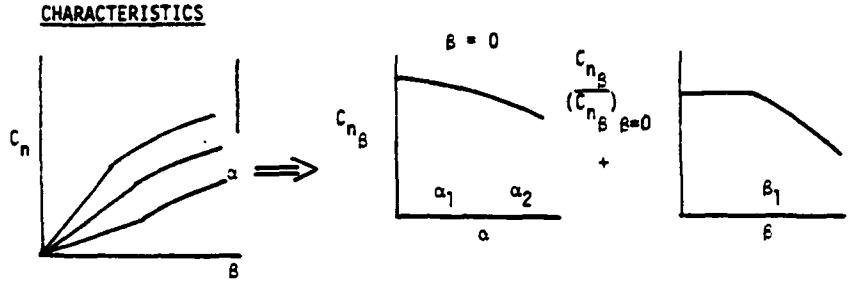

- α & ε SPLINE TERM DEFINITIONS

$$\Delta\alpha_i = \begin{cases} 0 & \text{IF } \alpha < \alpha_i \\ \alpha - \alpha_i & \text{IF } \alpha \geq \alpha_i \end{cases}$$

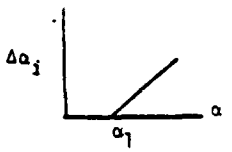

$$\Delta\alpha = \begin{cases} \varepsilon + \varepsilon_i & \text{IF } \beta < -\beta_i \\ 0 & \text{IF } |\beta| < \beta_i \\ \varepsilon - \varepsilon_i & \text{IF } \beta > \beta_i \end{cases}$$

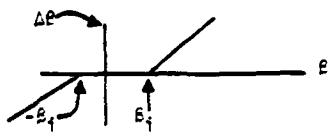

- SPLINE EQUATION

$$C_n = \underbrace{(K_{N1} + K_{N2}\,\alpha + K_{N3}\,\Delta\alpha_1 + K_{N4}\,\Delta\alpha_2)\beta}_{C_{n_\beta} \text{ FOR } \beta = 0} + \frac{K_{N5}\,\Delta\varepsilon}{\frac{C_{n_\beta}}{(C_{n_\beta})_{\beta=0}} - 1}$$

where

K_{N1} IS THE ESTIMATE OF C_{N_β} FOR $\alpha = \beta = 0$

K_{N2} IS THE ESTIMATE OF C_{N_ε} FOR $\alpha \neq 0$, $\varepsilon = 0$

K_{N3} CORRECTS THE ESTIMATE OF C_{N_ε} FOR $\alpha > \alpha_1$, $\varepsilon = 0$

K_{N4} CORRECTS THE ESTIMATE OF C_{N_ε} FOR $\alpha > \alpha_2$ $\varepsilon = 0$

K_{N5} CORRECTS THE ESTIMATE OF C_{N_β} FOR $\varepsilon \neq 0$

Figure 3.4. Spline Equation Formulation Example

variables. For example, to account for hysteresis, the inclusion of a spline term can be controlled by the value of $d\alpha/dt$.

3.3.1.2 Model Structure Data Processing

After the aerodynamic force and moment coefficients have been hypothesized, the next task is to determine which of the parameters are significant. This is done by reconstructing the aerodynamic force and moment coefficients from flight test measurements and then using an equation error identification algorithm to search for the most significant parameters. The following equation illustrates how an aerodynamic moment coefficient (C_n) is reconstructed from flight measurements:

$$C_n = \frac{1}{qS_w b_w} \left[I_z \frac{dR}{dt} - I_{xz} \left(\frac{dP}{dt} - QR \right) + (I_y - I_x)PQ \right]$$

q = dynamic pressure

S_w = wing area

b_w = wing span

P,Q,R = roll, pitch and yaw rates

$\frac{d}{dt}$ () = time derivative of ()

I_x, I_y, I_z = roll, pitch, yaw inertias

I_{xz} = product of inertia

It can be seen from this equation that if any of the flight measurements are biased or have a scale factor error, the reconstructed aerodynamic coefficient and the resulting model parameter estimates will also be biased.

An optimal subset regression (OSR) algorithm is used to identify the model structure from the reconstructed aerodynamic coefficient. OSR is an algorithm which adds and deletes variables to a particular model in an iterative manner. The algorithm uses

statistical hypothesis testing techniques based on the Fisher F ratio (e.g., F-tests). Formally, this ratio measures the difference in fit error with the current model relative to the error due to noise and model uncertainties. A "total" F-ratio measures the entire model fit relative to error and a "partial" F-ratio measures the incremental improvement in fit due to addition or deletion of a parameter in the model. A generalized flow chart is shown in Figure 3.5. Starting with a list of possible variables, the algorithm enters the first variable with the highest partial correlation to the observations y. The contribution of this variable to reducing the fit error is made, and a new variable entered. Subsequent tests add and delete variables to improve the "fit". The final subset of θ which results from the procedure is one within confidence bounds set by the user (say, 95 percent or 99 percent). The model structure selected from the OSR results is based on a consideration of two statistical figures of merit and a comparison of candidate model structures with wind tunnel and theoretical data. This comparison also provides a means to validate the selected model structure. The two statistical figures of merit are the multiple correlation coefficient (R^2) and the equation F ratio. For a perfect fit, $R^2 = 1$. Generally, $R^2 \rightarrow 1$ as additional terms are added to the model. The equation F ratio relates fit goodness to fit error weighted by the degrees of freedom of the model. The desired model is one that has a good fit $(R^2 \rightarrow 1)$ with the equation F ratio maximized.

3.3.2 T-2 Aerodynamic Formulation

Using the T-2 wind tunnel and theoretical aerodynamic data base (Chapter II) and the model hypothesis principles discussed in Section 3.3.1.1, generalized aerodynamic models were defined. The model for each of the aerodynamic force and moment equations is presented in Figure 3.6 with Table 3.2 containing a definition of terms from these equations. Modeling features are noted as follows:

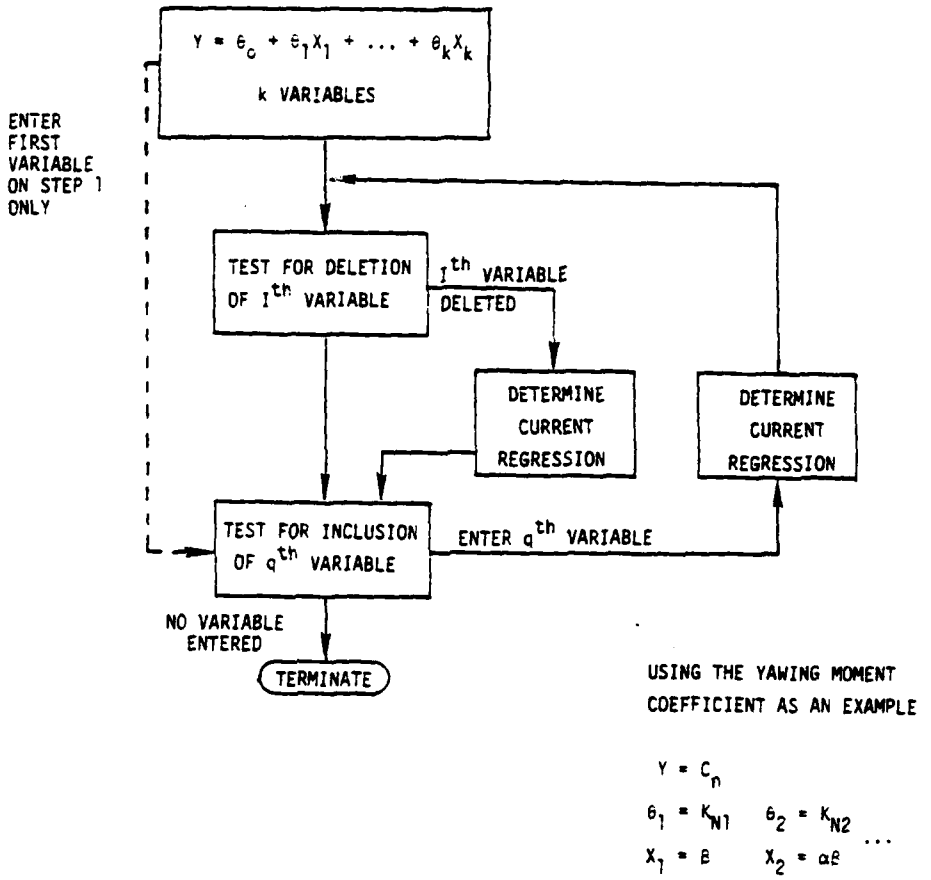

Figure 3.5. Optimal Subset Regression Program Flowchart

LONGITUDINAL AERODYNAMIC MODELS

LIFT EQUATION:

$$C_L = K_{L0} + K_{L1}\alpha + (K_{L2},K_{L3})\Delta\alpha_1 + (K_{L4},K_{L5})\Delta\alpha_2 + K_{L6}\Delta\alpha_2^2 + K_{L7}\Delta\alpha_3 + K_{L8}\Delta\alpha_3^2 + (K_{L9},K_{L10})\delta_e + K_{L11}|\delta_e|\delta_e + (K_{L12} + K_{L13} + K_{L14})\frac{\bar{c}Q_s}{2V_T} + (K_{L15} + K_{L16} + K_{L17})\frac{\bar{c}\,\dot{\alpha}}{2V_T} + K_{L18}|\beta| + K_{L19}|\beta|\alpha^2$$

DRAG EQUATION:

$$C_D = K_{D0} + K_{D1}\alpha^2 + (K_{D2},K_{D3})\Delta\alpha_1 + (K_{D4},K_{D5})\Delta\alpha_2 + K_{D6}|\delta_R| + K_{D7}\alpha^2|\delta_R| + K_{D8}|\beta| + K_{D9}\alpha^2|\beta|$$

PITCHING MOMENT EQUATION:

$$C_M = K_{M0} + K_{M1}\alpha + (K_{M2},K_{M3})\Delta\alpha_1 + (K_{M4},K_{M5})\Delta\alpha_2 + K_{M6}\Delta\alpha_3 + (K_{M7} + K_{M8} + K_{M9} + K_{M10})\delta_e + (K_{M11} + K_{M12} + K_{M13} + K_{M14})\frac{\bar{c}Q_s}{2V_T} + (K_{M15} + K_{M16} + K_{M17} + K_{M18})\frac{\bar{c}\,\dot{\alpha}}{2V_T} + K_{M19}|\delta_R| + K_{M20}\alpha^2|\delta_R| + K_{M21}|\beta| + K_{M22}\alpha^2|\beta|$$

NOTE: (K_{L2},K_{L3}) means that K_{L2} is the coefficient for $\dot{\alpha}>0$ and K_{L3} is the coefficient $\dot{\alpha}<0$

Figure 3.6. T-2 Aero Model Hypotheses

LATERAL-DIRECTIONAL MODELS

YAWING MOMENT EQUATION:

$$C_n = K_{N0} + K_{N1}\beta + K_{N2}\Delta\beta + K_{N3}\alpha\cdot\beta + K_{N4}\Delta\alpha_3\cdot\beta + K_{N5}\hat{P}_S + K_{N6}\hat{P}_S\cdot\alpha + K_{N7}\hat{P}_S\cdot\Delta\alpha_1 + K_{N8}\hat{P}_S\cdot\Delta\alpha_2 + K_{N9}\hat{P}_S\cdot\Delta\alpha_3$$
$$+ K_{N10}\hat{R}_S + K_{N11}\hat{R}_S\cdot\alpha + K_{N12}\hat{R}_S\cdot\Delta\alpha_1 + K_{N13}\hat{P}_S\cdot\Delta\alpha_2 + K_{N14}\hat{R}_S\cdot\Delta\alpha_3 + K_{N15}\delta_A + K_{N16}\delta_R + K_{N17}\delta_R\cdot\Delta\alpha_2 + K_{N18}\delta_R\cdot\Delta\alpha_3$$

ROLLING MOMENT EQUATION:

$$C_\ell = K_{R0}\beta + K_{R1}\Delta\beta + K_{R2}\alpha\cdot\beta + K_{R3}\Delta\alpha_2\cdot\beta + K_{R4}\hat{P}_S + K_{R5}\hat{P}_S + K_{R6}\hat{P}_S\cdot\alpha_1 + K_{R7}\hat{P}_S\cdot\Delta\alpha_2 + K_{R8}\hat{P}_S\cdot\Delta\alpha_3 + K_{R9}\hat{R}_S$$
$$+ K_{R10}\hat{R}_S\cdot\alpha + K_{R11}\hat{R}_S\cdot\Delta\alpha_1 + K_{R12}\hat{R}_S\cdot\Delta\alpha_2 + K_{R13}\hat{R}_S\cdot\Delta\alpha_3 + K_{R14}\delta_a + K_{R15}\delta_a + K_{R16}\delta_a\cdot\Delta\alpha_1 + K_{R17}\delta_a\cdot\Delta\alpha_2$$
$$+ K_{18}\delta_a\cdot\Delta\alpha_3 + K_{R19}\delta_R + K_{R20}\alpha\delta_R + K_{R21}\Delta\alpha_1\delta_R$$

SIDE FORCE EQUATION:

$$C_Y = K_{Y0} + K_{Y1}\beta + K_{Y2}\Delta\beta + K_{Y3}\hat{P}_S + K_{Y4}\hat{R}_S + K_{Y5}\delta_R$$

Figure 3.6. (Concluded)

TABLE 3.2. AERODYNAMIC MODEL VARIABLES

1. ANGLE OF ATTACK SPLINES

$$\Delta\alpha_1 = \alpha - \alpha_1 \geq 0$$

$$\Delta\alpha_2 = \alpha - \alpha_2 \geq 0$$

$$\Delta\alpha_3 = \alpha - \alpha_3 \geq 0$$

where $\alpha_1 = 0.1745$ rad (10°)

$\alpha_2 = 0.2793$ rad (16°)

$\alpha_3 = 0.3840$ rad (22°)

2. SIDESLIP SPLINE

$$\Delta\beta = \begin{cases} \beta - \beta_1 & \text{IF } \beta > \beta_1 \\ 0 & \text{IF } |\beta| \leq \beta_1 \\ \beta + \beta_1 & \text{IF } \beta < \beta_1 \end{cases}$$

3. NORMALIZED ROTATIONAL RATES

$$\hat{P}_s = \frac{bwP}{2V_T S} = \frac{bw}{2V_T} (\cos\alpha\, P - \sin\alpha\, R)$$

$$\hat{Q}_s = \frac{\bar{c}wQ}{2V_T S} = \frac{\bar{c}wQ}{2V_T}$$

$$\hat{R}_s = \frac{bwR}{2V_T S} = \frac{bw}{2V_T} (\sin\alpha\, P + \cos\alpha\, R)$$

(1) Nonlinearities in α and β were incorporated with spline terms. Some of the α spline terms in the lift and pitching moment equations are defined separately for airplane nose up and down maneuvers.

(2) The vertical plane force coefficients are modeled by lift (C_L) and drag (C_D) instead of axial (C_X) and normal (C_N) force coefficients since the curve shape for (C_D is much simplier than that for C_X.

(3) The equations included cross axis coupling terms. The lift-drag and pitching moment models included sideslip and rudder deflection. The yawing moment-rolling moment and sideforce equations are dependent on angle-of attack.

The aerodynamic models described in Figure 3.6 were implemented in the OSR algorithm and the flight measurements for the test conditions described in Table 2.3 were processed. Since these flight conditions represented different kinds of maneuvers, the most significant model structure, as defined by OSR, varied from run to run. Table 3.3 shows the correlation coefficients obtained for each equation and flight condition. Its apparent that the information content of some maneuvers was much better than that for others. Also the models for C_n were worse than those for the other force and moment equations. The problem in modeling C_n is that the yaw rate measurement, which is used to reconstruct C_n, was a poor signal (see Section 3.1). By interpreting the OSR results with much engineering judgment, the results were combined to produce composite longitudinal and lateral-directional models. These are presented in Tables 3.4 and 3.5.

3.3.3 Model Structure Validation

The selected aerodynamic models were validated by comparison to wind tunnel data and theoretical prediction. Figures 3.7 to 3.12 show the results of this comparison.

Figures 3.7 to 3.9 show C_L, C_m, and C_D. Of interest in these curves, particularly in C_L, is an aerodynamic hysteresis detected

TABLE 3.3. STATISTICAL SIGNIFICANCE OF MODEL STRUCTURE DETERMINATION[a]

	AERODYNAMIC COEFFICIENT					
	C_L	C_D	C_m	C_l	C_n	C_Y
δ_e RAMP + SINE	.56	.98	.85	.72	.06	.94
δ_e AFT + PULSES	.19	.74	.94	.58	.04	.80
LIMIT CYCLE	.68	.96	.98	.18	.03	.24
δ_e DOUBLET	.97	.98	.96	.60	.12	.77
δ_e RANDOM	.96	.98	.96	.78	.18	.61
δ_A RANDOM	.80	.82	.59	.99	.66	.74
SEQUENTIAL DOUBLETS	.97	.98	.94	.99	.82	.98
δ_R RANDOM	.77	.84	.74	.96	.84	.99
SEQ. RANDOM, β_T=0°	.96	.96	.96	.68	.19	.46
SEQ. RANDOM, β_T=-5°	.81	.94	.92	.91	.48	.85
SEQ. RANDOM, β_T=5°	.88	.94	.94	.91	.55	.81
δ_e AFT, FULL δ_R	.86	.96	.93	.83	---	.96
δ_e AFT, FULL δ_a	.72	.93	.94	.48	.04	.91
SHALLOW BANK TO STALL	.48	.98	.84	.71	.08	.88
STEEP BANK TO STALL	.89	.98	.90	.65	.20	.91
PULL-UP TO STALL	.95	.97	.87	.61	.22	.92
CO-ORD. SPIN ENTRY	.80	.96	.84	.76	.17	.91

[a]Variance explained by R^2(R^2 = 1 is a perfect explanation).

TABLE 3.4. IDENTIFIED LONGITUDINAL MATH MODEL STRUCTURES

LIFT COEFFICIENT:

$$C_L = .04 + 5.19\alpha + \begin{bmatrix} -1.69_{(\dot{\alpha}>0)} \\ -3.67_{(\dot{\alpha}<0)} \end{bmatrix} \Delta\alpha_1 + \begin{bmatrix} -5.61_{(\dot{\alpha}>0)} \\ -1.62_{(\dot{\alpha}<0)} \end{bmatrix} \Delta\alpha_2 + 6.0\Delta\alpha_3^2 - .24|\beta| + .31\delta_e$$

DRAG COEFFICIENT:

$$C_D = -.031 + 3.13\alpha^2 + \begin{bmatrix} .146_{(\dot{\alpha}>0)} \\ -.139_{(\dot{\alpha}<0)} \end{bmatrix} \Delta\alpha_1 + \begin{bmatrix} -.28_{(\dot{\alpha}>0)} \\ 0_{(\dot{\alpha}<0)} \end{bmatrix} \Delta\alpha_2 - .0057|\beta| + .0741|\delta_R| + 1.00\delta_e^2$$

PITCHING MOMENT COEFFICIENT:

$$C_m = .072 - .95\alpha + \begin{bmatrix} -.22_{(\dot{\alpha}>0)} \\ -.59_{(\dot{\alpha}<0)} \end{bmatrix} \Delta\alpha_1 + \begin{bmatrix} .39_{(\dot{\alpha}>0)} \\ 1.28_{(\dot{\alpha}<0)} \end{bmatrix} \Delta\alpha_2 - 1.00\Delta\alpha_3 - .136|\beta| + .097|\delta_R| + C_{m_q}\left(\frac{\bar{c}Q}{2V_T}\right) + C_{m_{\delta e}}\delta e$$

where

$$C_{m_q} = \begin{cases} -9.42 & \text{if } \alpha<\alpha_1 \\ -.51 & \text{if } \alpha_1<\alpha<\alpha_2 \\ -3.65 & \text{if } \alpha_2<\alpha<\alpha_3 \\ -7.08 & \text{if } \alpha>\alpha_3 \end{cases}, \qquad C_{m_{\delta e}} = \begin{cases} -1.03 & \text{if } \alpha<\alpha_1 \\ -.95 & \text{if } \alpha_1<\alpha<\alpha_2 \\ -.78 & \text{if } \alpha>\alpha_2 \end{cases}$$

TABLE 3.5. IDENTIFIED LATERAL-DIRECTIONAL MODEL STRUCTURES

YAWING MOMENT COEFFICIENT:

$$C_n = (.086 - .122\alpha + .122\Delta\alpha_3)\beta + (-.0537 + 2.865\Delta\alpha_2 - 2.865\,\Delta\alpha_3)\left(\frac{Pb}{2V_T}\right) + (-.13 - .172\alpha + .172\Delta\alpha_1)\left(\frac{Rb}{2V_T}\right)$$
$$+ (-.0526 + .656\Delta\alpha_2 - .656\Delta\alpha_3)\delta_R$$

ROLLING MOMENT COEFFICIENT:

$$C_\ell = (-.079 - .248\alpha + .248\Delta\alpha_2)\beta + .079\Delta\beta + (-.502 - .69\alpha + 5.85\Delta\alpha_1 - 5.16\Delta\alpha_2)\left(\frac{Pb}{2V_T}\right) + .292\left(\frac{Rb}{2V_T}\right)$$
$$+ (-.38\alpha + .19\Delta\alpha_1)\delta_R + (-.212 + .23\alpha)\,\delta_A$$

SIDE FORCE COEFFICIENT:

$$C_y = -.338\beta - .359\Delta\beta + .115\delta_R$$

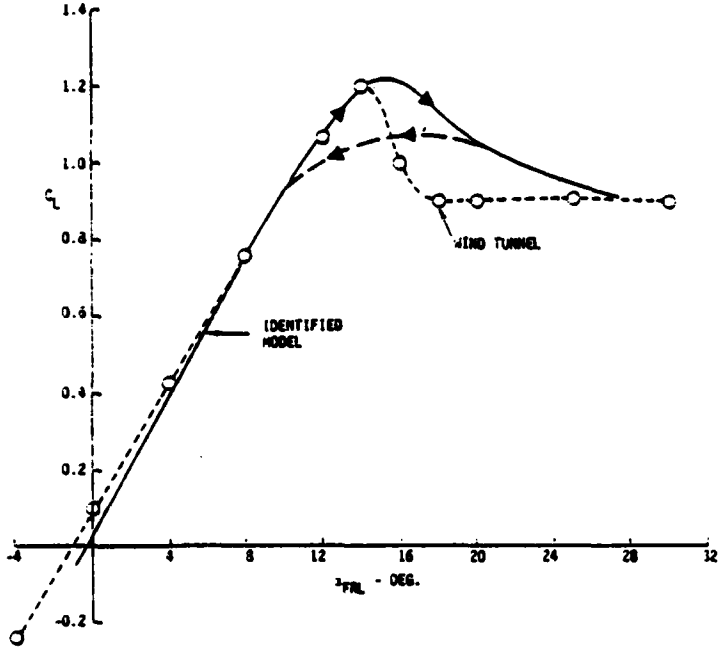

Figure 3.7. Lift Coefficient Variation with Angle of Attack

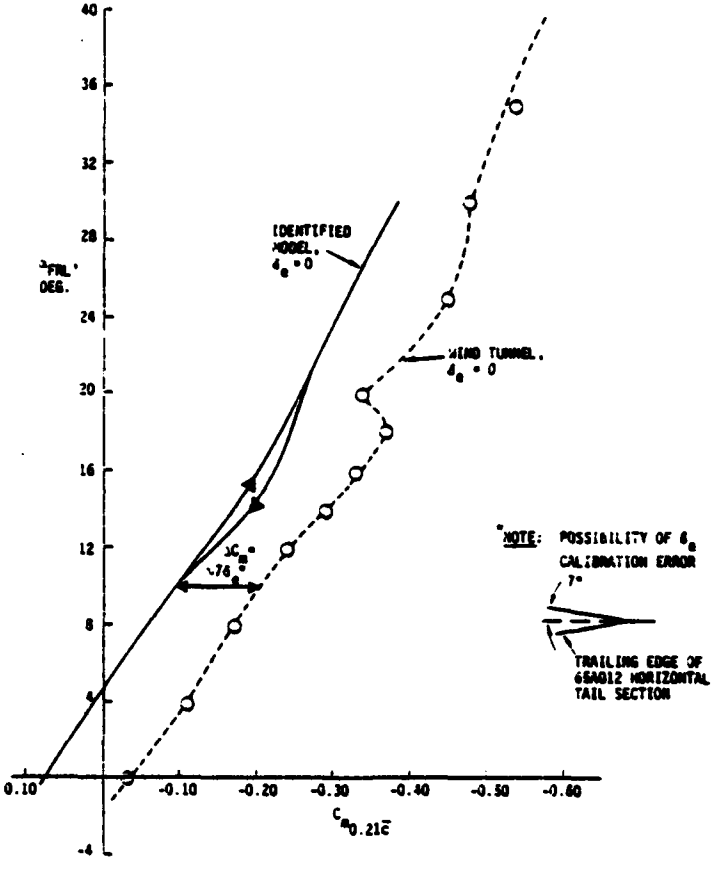

Figure 3.8. Pitching Moment Coefficient Variation with Angle of Attack

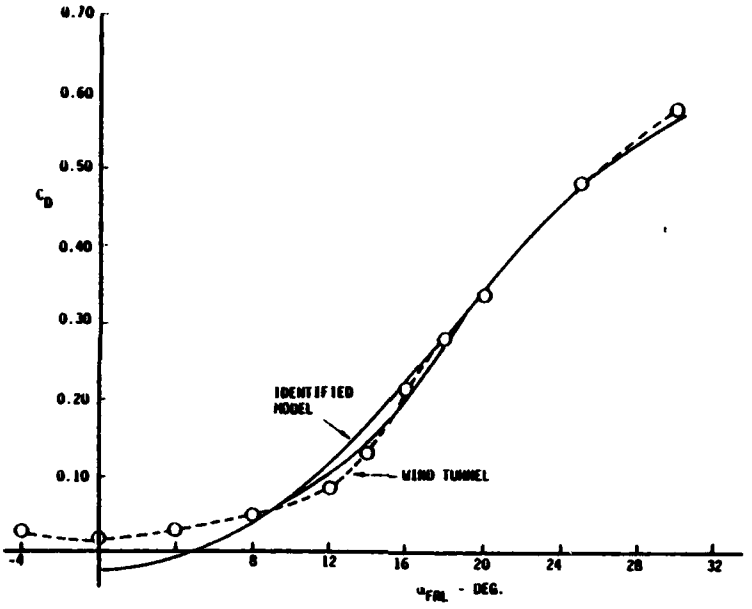

Figure 3.9. Drag Coefficient Variation with Angle of Attack

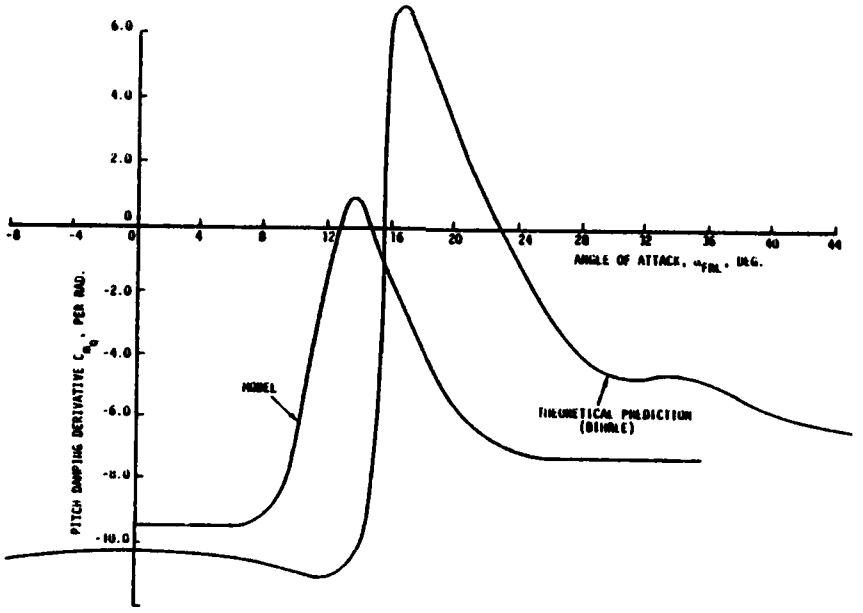

Figure 3.10. Variation of C_{m_q} with Angle of Attack

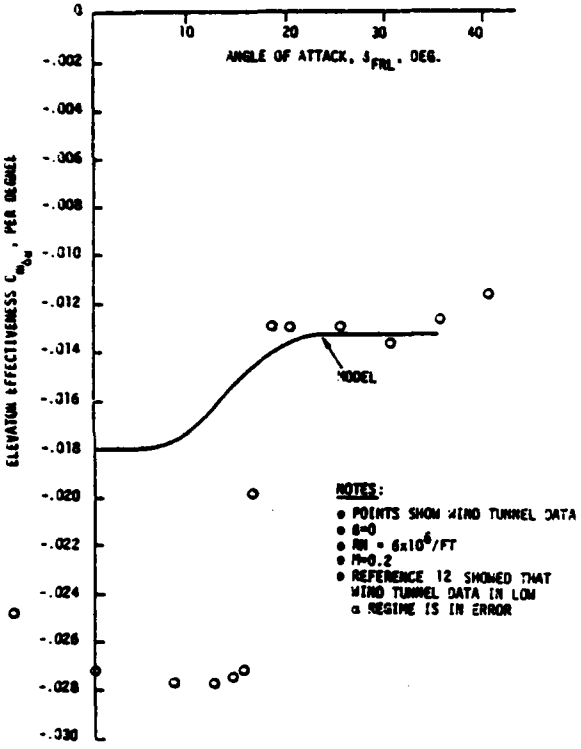

Figure 3.11. Variation of Elevator Effectiveness with Angle of Attack

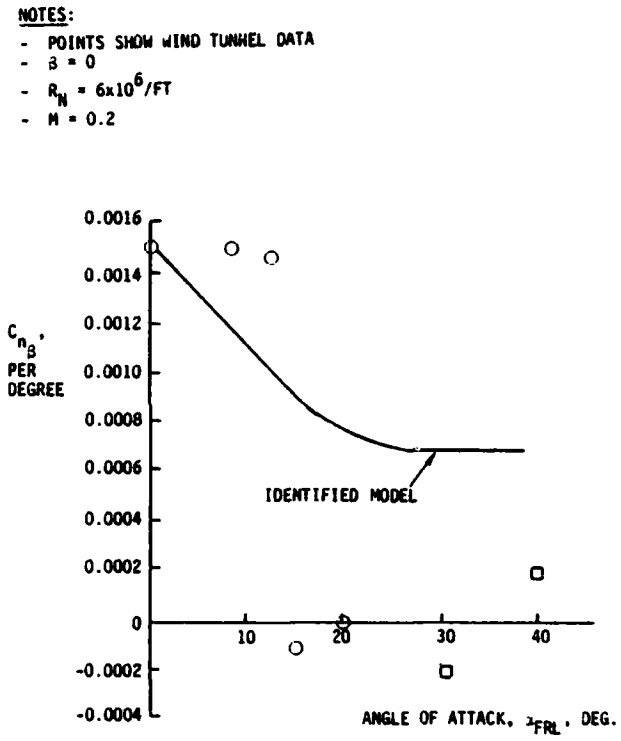

Figure 3.12. Variation of C_{n_β} with Angle of Attack

by allowing the coefficients of $\Delta\alpha$ to assume different values depending on whether pitch rate was positive or negative. This effect is in general agreement with previous studies of hysteresis but it is believed that this is the first time it has been identified from flight data. The lift deficit causes a similar shift in C_m over the same α range.

The C_m results, Figure 3.8, show that static stability C_{m_α}, has been closely identified. An offset in trim angle of attack may be caused by an elevator calibration error, as show on the figure. The pitching moment pitch up at $\alpha \approx 20^0$, likely due to wing-tail interference, was not identified due to the limited number of spline segments available.

Drag correlation, shown in Figure 3.9, was hampered by lack of data on engine thrust level. This is needed because the net X-axis force, T-D, is identified from acceleration data, and thrust must be known to determine drag. In this case, the thrust was computed from estimated drag in the trim condition, using wind tunnel data. More accurate a_x instrumentation, engine parameter instrumentation (e.g., RPM), and models for installed thrust are required in order to precisely define the shape of the drag polar.

Figures 3.10 to 3.22 show other control effectiveness, aerodynamic damping, and aerodynamic force coefficients and derivatives identified from flight data, compared to values from other sources. In general, identified values were used in preference to other data, unless levels of confidence were very low.

Figures 3.14 and 3.15 show in detail the agreement between the nonlinear models and wind tunnel data, for C_ℓ and C_n as functions of β at various values of α. The agreement is, in general, quite good.

Figures 3.7 to 3.21 show the forms in which starting parameter values were input to the nonlinear maximum likelihood parameter

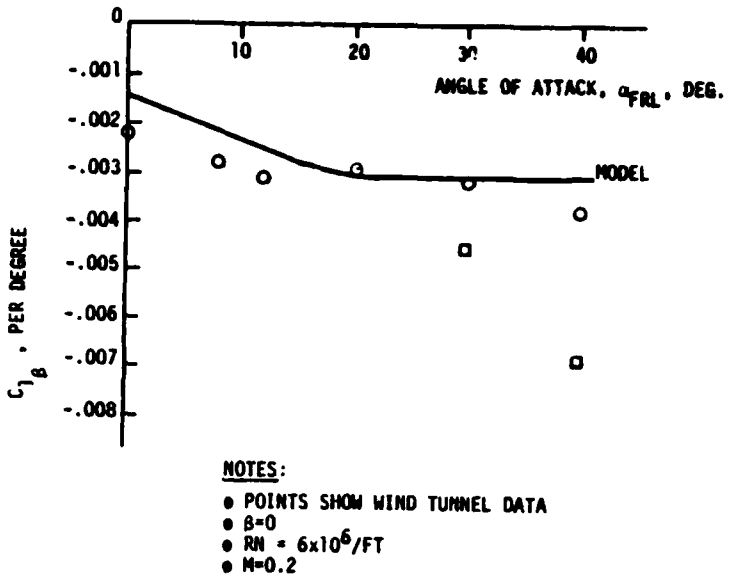

Figure 3.13. Variation of C_{l_β} with Angle of Attack

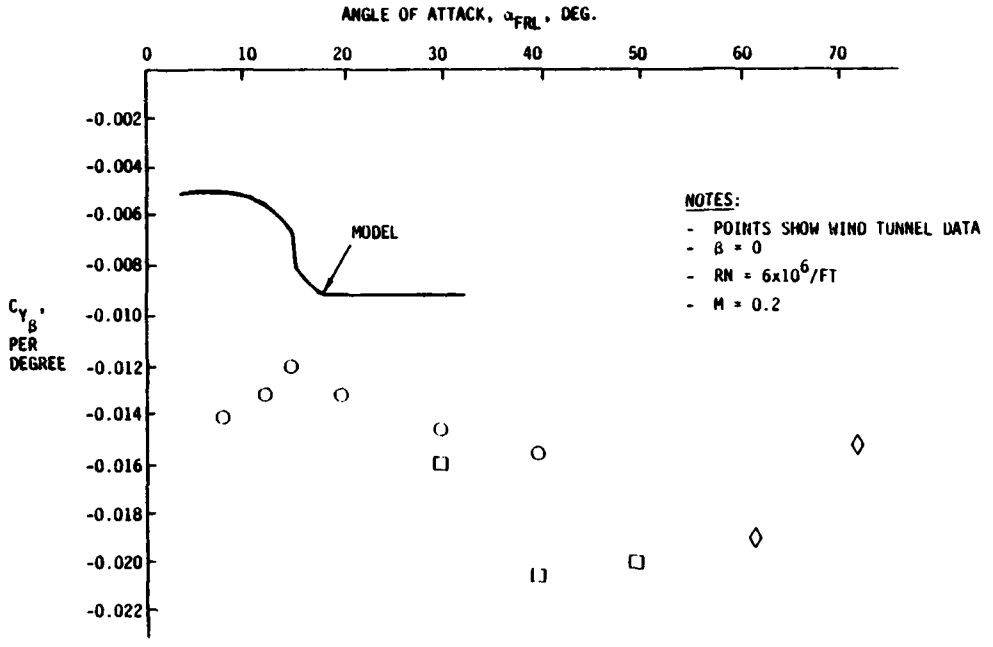

Figure 3.14. Variation of C_{Y_β} with Angle of Attack

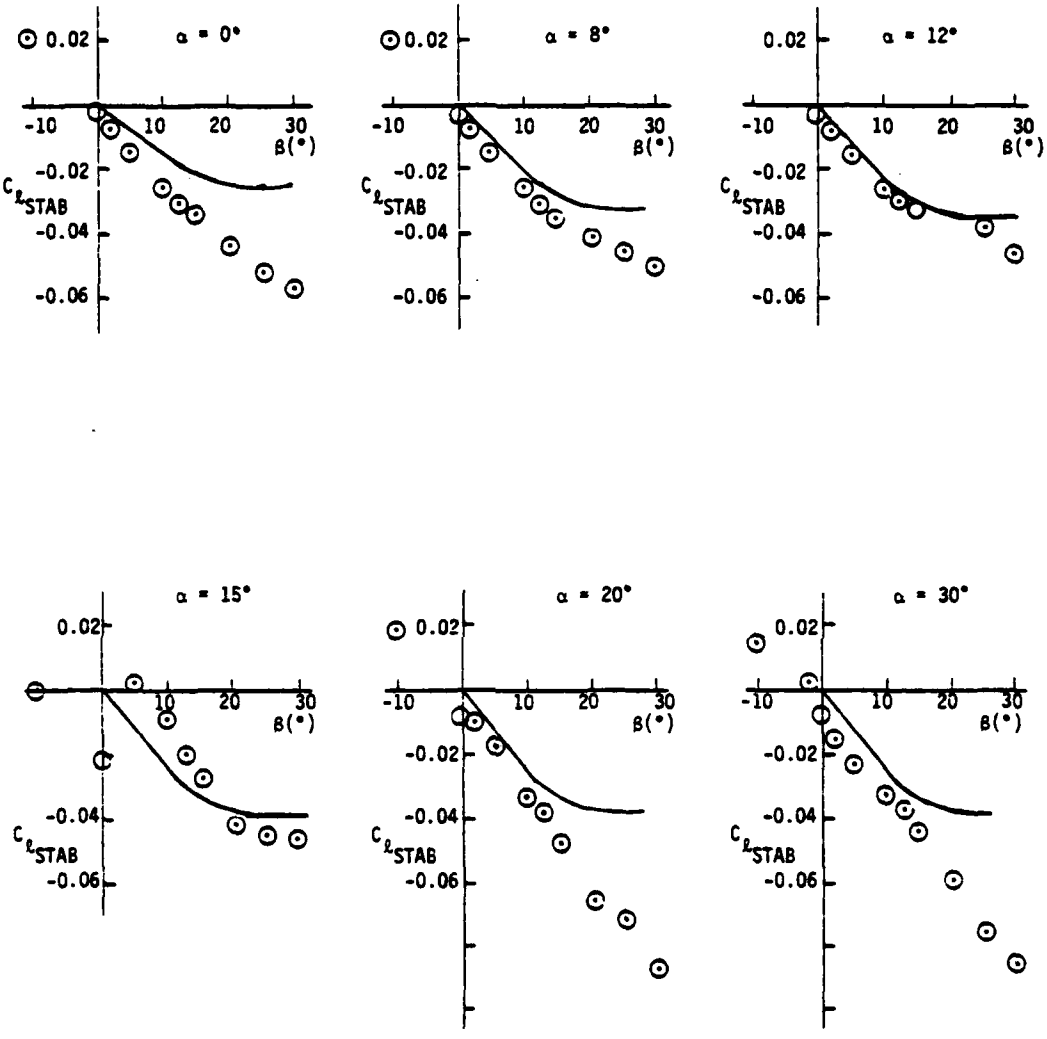

Figure 3.15. Comparison of Model to Wind Tunnel Data

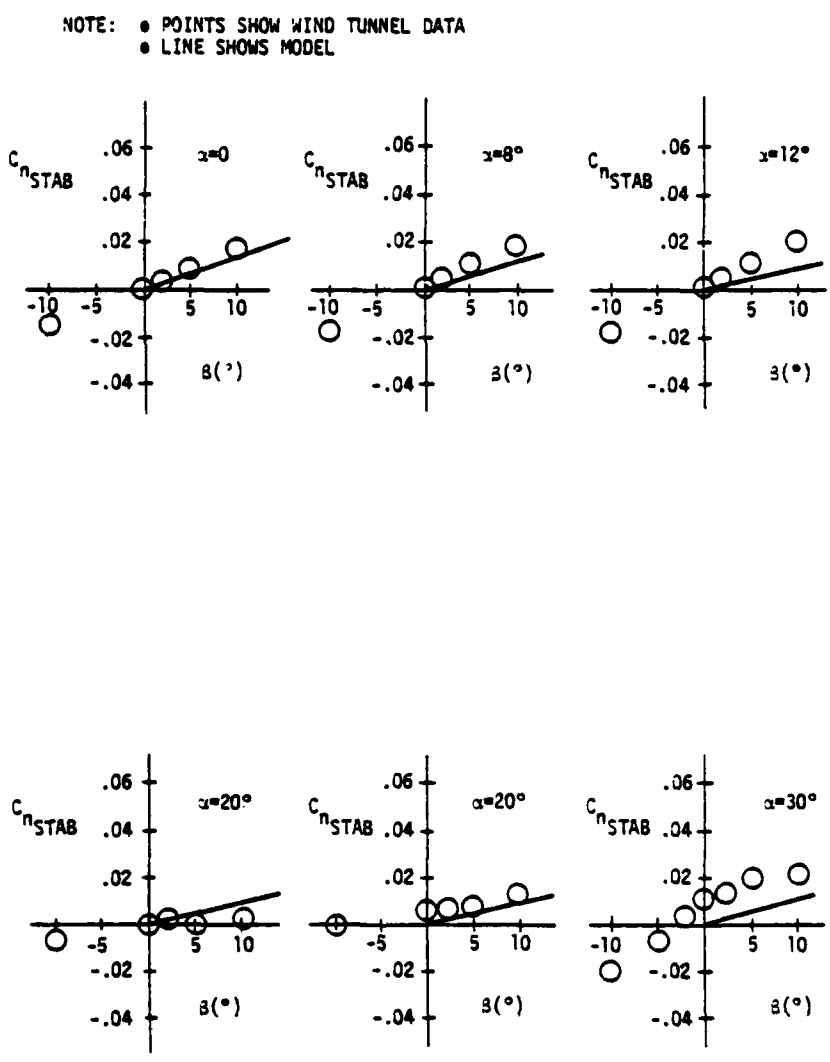

Figure 3.16. Comparison of Yawing Moment Coefficient

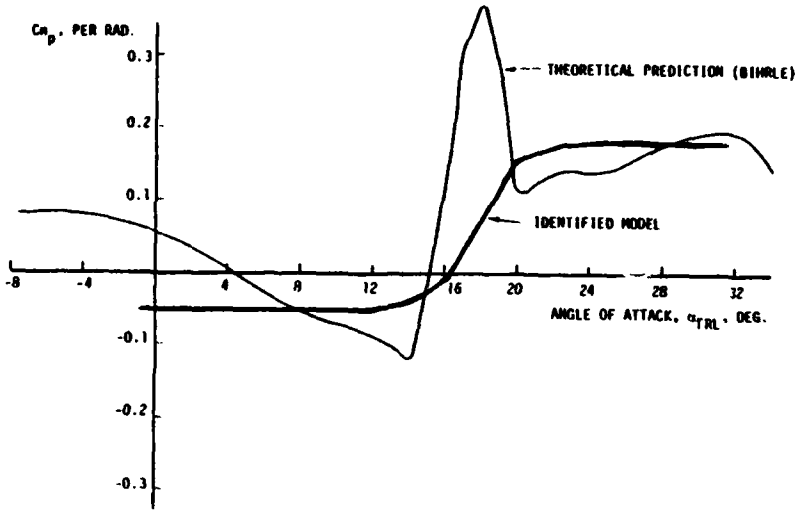

Figure 3.17. Variation of C_{n_p} with Angle of Attack

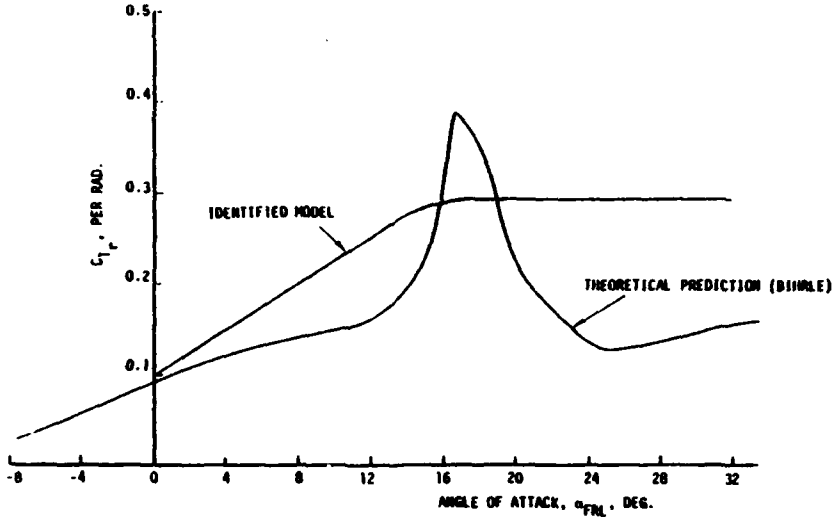

Figure 3.18. Variation of C_{l_r} with Angle of Attack

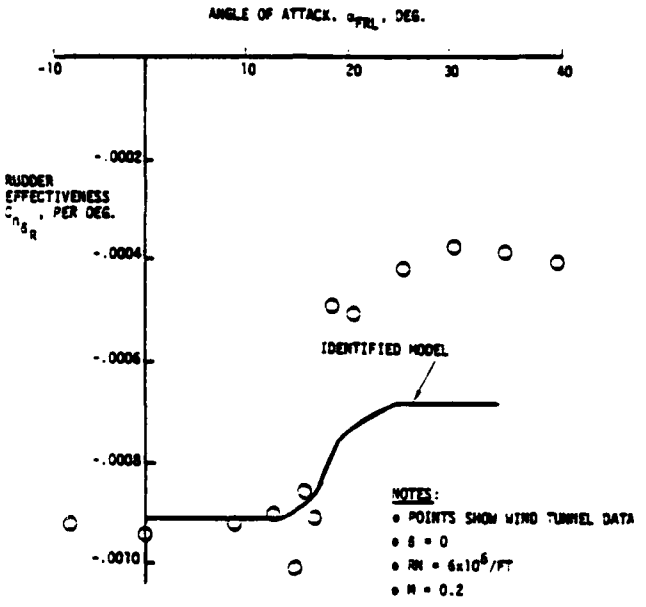

Figure 3.19. Variation of Rudder Effectiveness with Angle of Attack

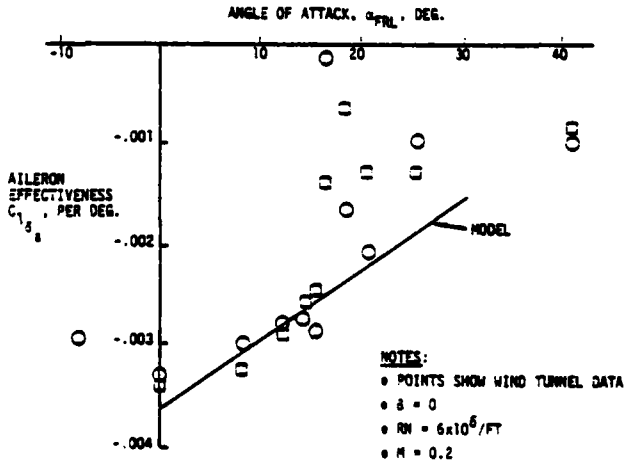

Figure 3.20. Variation of Aileron Effectiveness with Angle of Attack

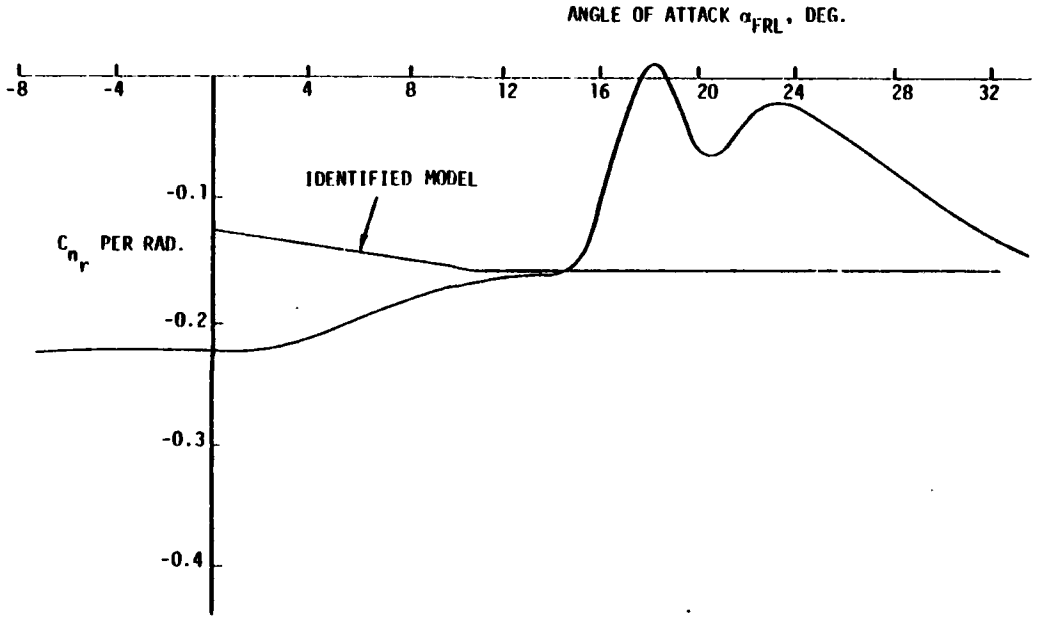

Figure 3.21. Variation of C_{n_r} with Angle of Attack

identification program. Specific spline regions were called out for which this program would attempt to obtain improved parameter values, in the sense of improved overall model fit. The results of this investigation are discussed in the following section.

3.4 PARAMETER IDENTIFICATION AND VERIFICATION

3.4.1 Approach

Two operations are now performed with the aerodynamic coefficients determined above: (1) the coefficients are used as starting values in a maximum likelihood parameter estimation analysis searching for improved estimate values; and (2) dynamic time histories are generated from the model equations and compared to the measurements, giving an indication of model fidelity.

The 6 degree of freedom model is divided into the customary 3 DOF longitudinal and lateral-directional models in order to simplify error interpretation and reduce the number of parameters to be identified at one time. Lateral-directional variables are supplied by lateral-directional measurements read in during the solution of the longitudinal equations of motion. This does not prohibit the estimation of coupling derivatives, such as the dependence of a longitudinal parameter on a lateral-directional degree of freedom, C_{L_β}, for example, since β is read in to the longitudinal equations in the same manner as a control deflection.

Several runs were selected for further analysis, based on the range of α and β available and on the general quality of the correlation coefficient characteristics established during the model structure determination phase of the study (see Table 3.3). The runs selected are, for the longitudinal case, the random elevator and elevator doublet maneuvers, and for the lateral-directional case the random aileron maneuver. The former longitudinal maneuver was used for identification, the latter for a prediction test, the "acid test" of a model; the lateral-directional maneuver was used for identification only, due to generally poorer measurement data quality (see Section 3.2.4).

The criteria employed in model fidelity analysis are both qualitative and quantitative. Obviously, a perfect time history match on a prediction run is indicative of a good model. Recall that a prediction run is one in which the control inputs from one maneuver, say B, are applied to the math model derived from another maneuver, say A, and the resulting model motion calculations compared to the actual behavior of B. If perfect agreement is seen, the model has been shown to be general and not the result of a unique convergence to data from a particular maneuver.

The identification process yields calculations of both noise covariance, or dispersion about the mean, and model error covariance, or the difference between the model predictions and the measured data. Statistical results showing large error covariances are often very apparent in poor time history matches of a given degree of freedom.

The results in the next two subsections illustrate the type of treatment employed in this study, and the results obtained.

3.4.2 Longitudinal Results

Model parameter values obtained from the model structure determination process were used as starting values to the maximum likelihood parameter estimation program SCIDNT and improved estimation of selected parameters was sought. The level of improvement was evaluated by comparing model error covariance magnitudes before and after the operation, and by time history comparisons of the final model to the measured data.

The initial longitudinal model parameters were shown in Table 3.4. Data from the random elevator maneuver (see Figures 3.22-3.26) were processed for model identification. The improvement in the model resulting from running the maximum likelihood program is seen by comparing the initial model error covariances with the final error covariances, as shown in Table 3.6. These values, computed from time history comparisons of model estimates of the measurements versus actual data, show that the model fit is much improved after the adjustment of parameter values.

NOTES:

1) δ_e RANDOM MANEUVER
2) NUMBERS ON THE PLOT SHOW THE NUMBER OF DATA POINTS FOR INDICATED α/β REGION

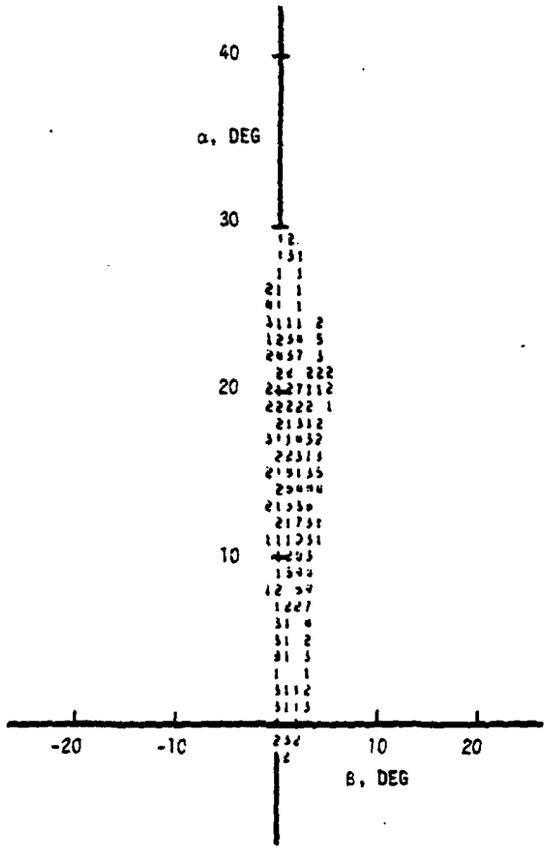

Figure 3.22. α/β Histogram for Longitudinal Model Identification

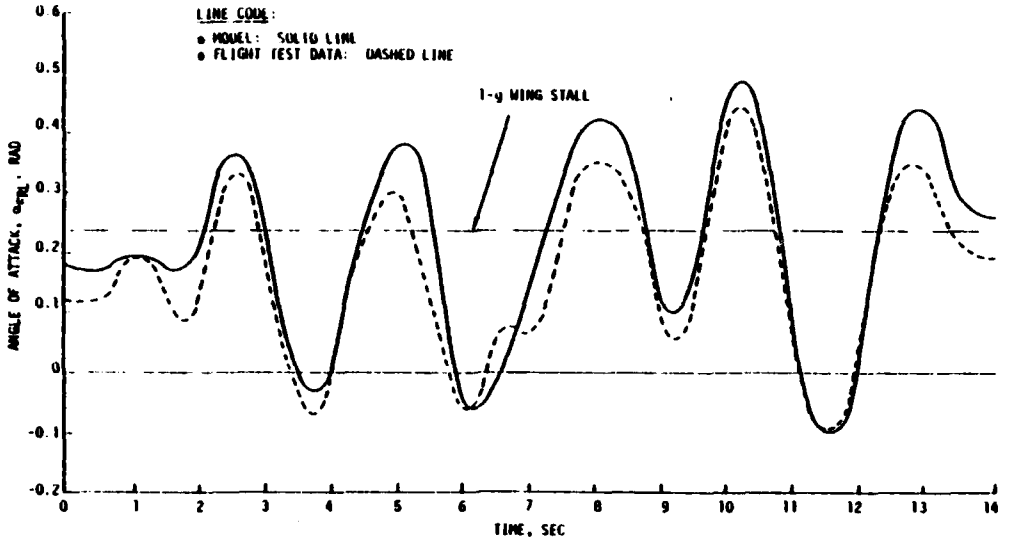

Figure 3.23. Model Identification δ_e Random Input: Angle of Attack

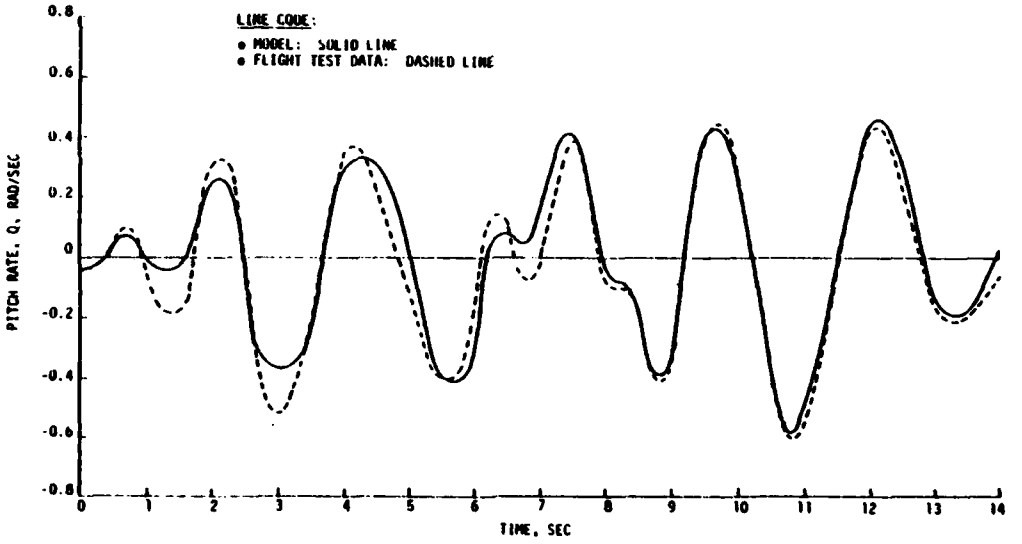

Figure 3.24. Model Identification δ_e Random Input: Pitch Rate

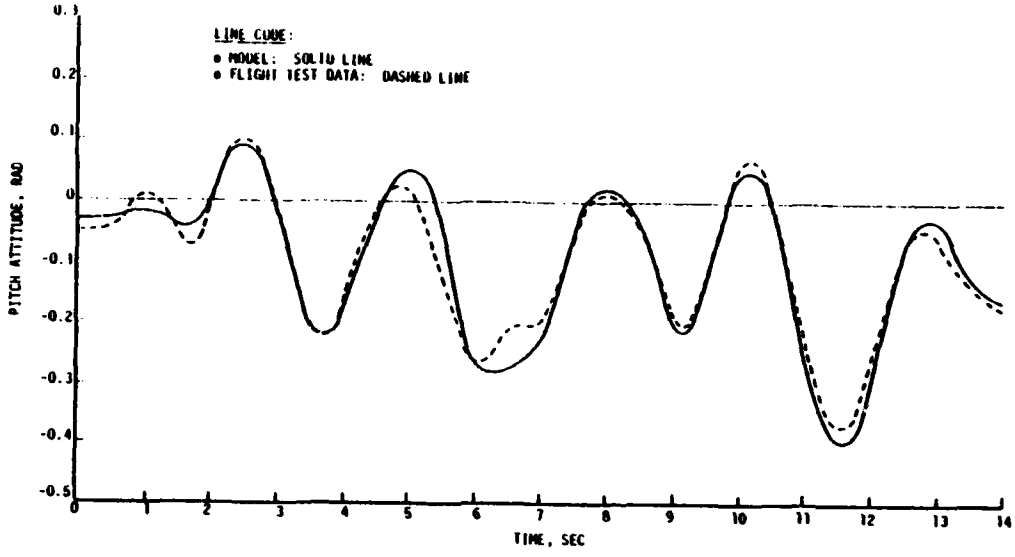

Figure 3.25. Model Identification δ_e Random Input: Pitch Attitude

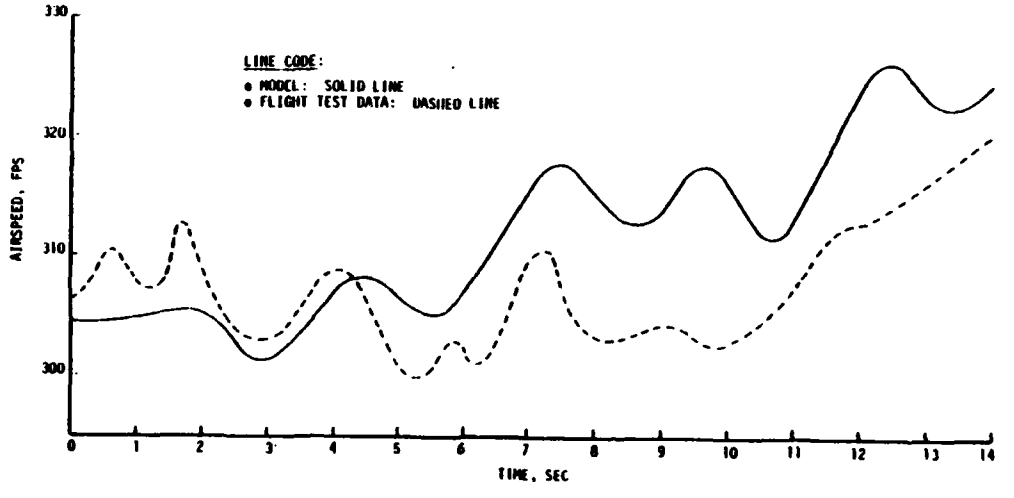

Figure 3.26. Model Identification δ_e Random Input: Airspeed

TABLE 3.6. MEASUREMENT MEAN SQUARE ESTIMATION ERROR: RANDOM ELEVATOR MANEUVER

α ~ rad
V ~ fps
Q ~ rad/sec
θ ~ rad

INITIAL

	α	V	Q	θ
α	.0255	0	0	0
V	0	97.6	0	0
Q	0	0	.0085	0
θ	0	0	0	.0625

WITH PARAMETER VALUES FROM MODEL STRUCTURES DETERMINATION ANALYSIS

FINAL

	α	V	Q	θ
α	.00323	0	0	0
V	0	60.75	0	0
Q	0	0	.0065	0
θ	0	0	0	.00072

WITH MAX. LIKELIHOOD IMPROVEMENT

	σ
α	.0568 rad
V	7.79 fps
Q	.0806 rad/sec
θ	.027 rad

The angle-of-attack time history, Figure 3.23, shows good agreement on frequency and amplitude over the duration of the maneuver. Deviations near peak amplitude contribute the most toward rms error (σ), and small differences in phase appear as large differences in magnitude. Therefore, the overall fit appears better than the $\sigma_\alpha = 3.26^0$ value might imply.

The agreement in pitch rate, Figure 3.24, an important pilot cue and handling qualities determinant, is excellent. Elevator effectiveness and short-period-related aerodynamic parameters appear to have been well identified. Again the $\sigma_Q = 4.62^0$ /sec value is misleading relative to the adequacy of the fit.

It is concluded here that simple measures of fit accuracy, such as standard deviation, are unreliable for judging models, and must be accompanied by engineering judgment and more comprehensive statistical criteria, such as correlation.

Pitch attitude, Figure 3.25, also shows excellent agreement throughout the maneuver. The agreement found with velocity, Figure 3.26, is not good, and is in fact worse than $\sigma_V = 7.8$ fps might imply. The generally poor quality of longitudinal accelerometer data is held responsible for this lack of agreement.

The conclusion is that the model determined in general form by regression analysis of numerous maneuvers, then refined by the parameter identification program, predicts aircraft behavior very well in the nonlinear, post-stall flight regime, as evidenced by the results of this first maneuver analysis. To test model generality, a second maneuver was selected, also with a wide angle-of-attack range, as shown in its histogram, Figure 3.27, but more in the linear below-stall regime. The same model, with the control inputs of the new maneuver, produced the error statistics shown in Table 3.7 and the time history comparisons shown in Figures 3.28 through 3.31.

Again, time history comparisons are found to be very good. Angle-of-attack and pitch rate show well-modeled short period

NOTES:

1) δ_e DOUBLET MANEUVER
2) NUMBERS ON THE PLOT SHOW THE NUMBER OF DATA POINTS FOR INDICATED α/β REGION

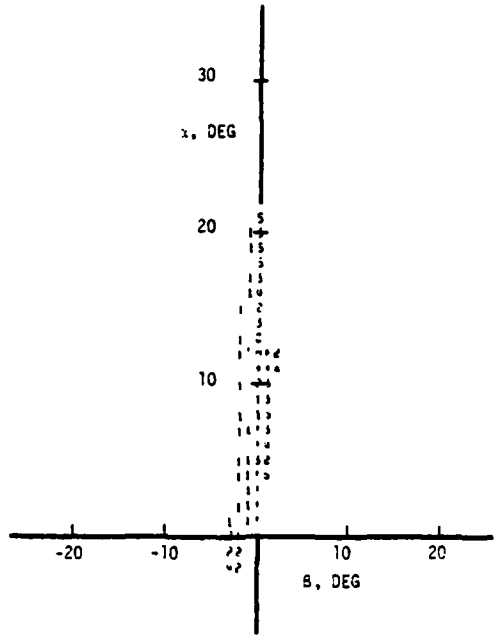

Figure 3.27. α/β Histogram for First Longitudinal Model Prediction Maneuver

TABLE 3.7. MEASUREMENT MEAN SQUARE ESTIMATION ERROR: ELEVATOR DOUBLET MANEUVER

x	.00172	0	0	0	α	.041 rad
V	0	22.43	0	0	V	4.74 ft/sec
Q	0	0	.00547	0	Q	.074 rad/sec
θ	0	0	0	.00164	θ	.040 rad

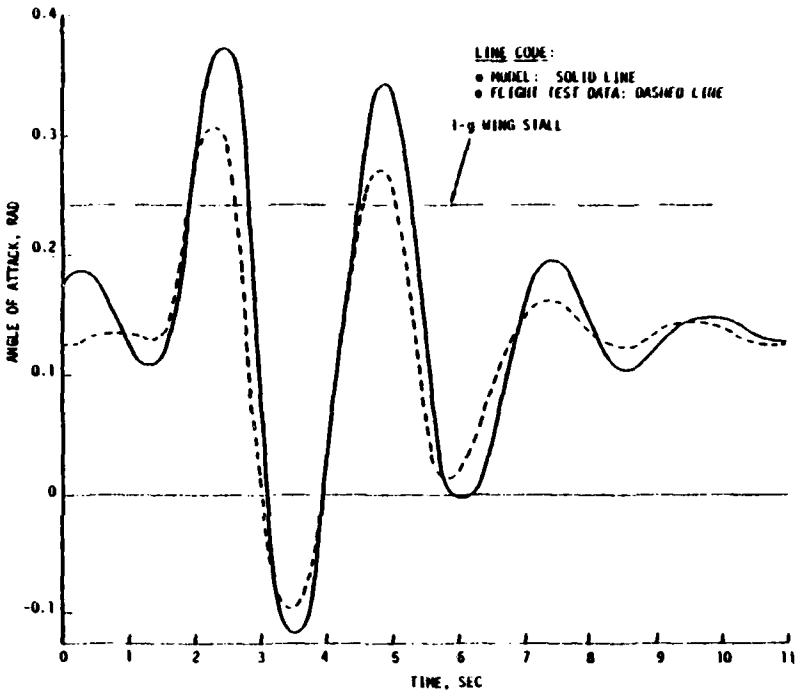

Figure 3.28. Prediction of δ_e Doublet Maneuver with δ_e Random Model: Angle of Attack

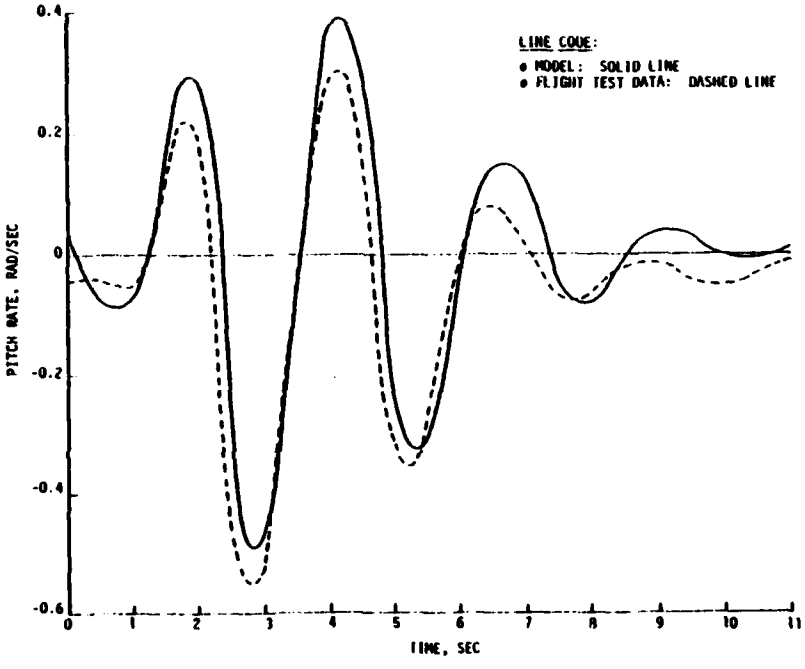

Figure 3.29. Prediction of δ_e Doublet Maneuver with δ_e Random Model: Pitch Rate

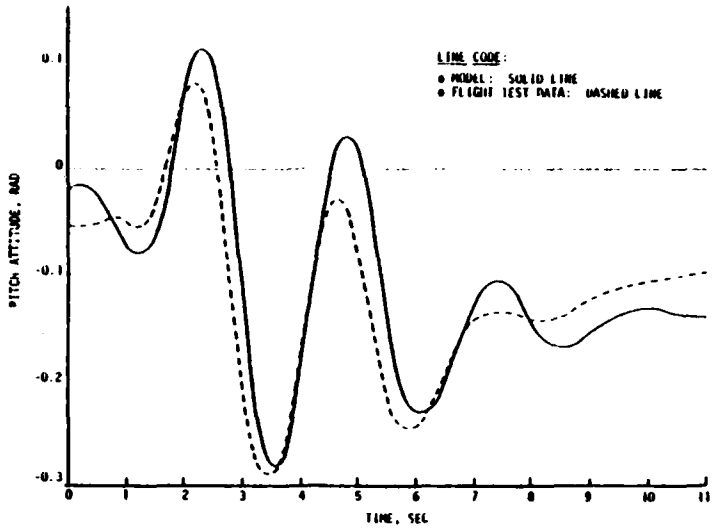

Figure 3.30. Prediction of δ_e Doublet Maneuver with δ_e Random Model: Pitch Attitude

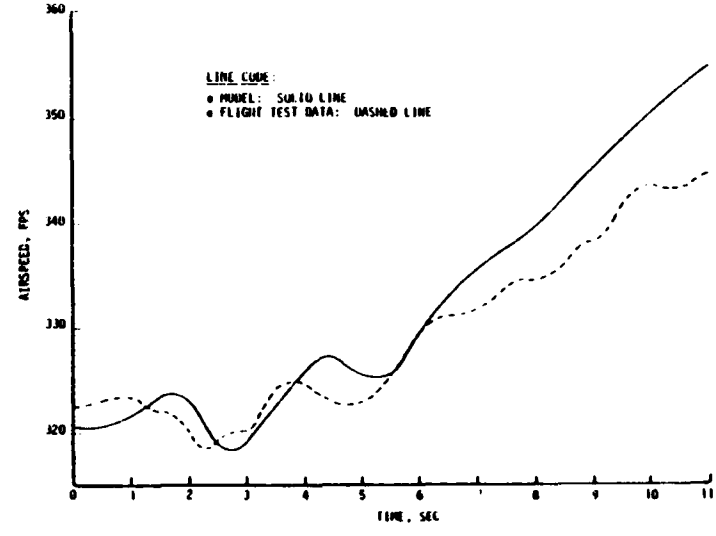

Figure 3.31. Prediction of δ_e Doublet Maneuver with δ_e Random Model: Airspeed

and control response characteristics; pitch attitude, accordingly, is good; and velocity, still the poorest, shows the proper trend and is close on response frequency.

To further test the validity of this longitudinal model, a maneuver with large excursions in both angle of attack and sideslip was selected for comparison. Before computing time histories, the sideslip information was processed in an identification mode to refine estimates of β-dependent parameters. A histogram of this maneuver, showing α and β excursions, is shown in Figure 3.32. Figures 3.33 through 3.36 show the time history comparisons for this case. Again, though peak amplitudes are underpredicted, fair agreement between model and measurement is seen.

The conclusion reached from this longitudinal analysis is that a general model has been developed in the approach described, that gives results with accuracy adequate for simulating piloted handling qualities in the nonlinear, high-α regime.

3.4.3 Lateral-Directional Results

The lateral-directional parameters identified by regression analysis were shown in Table 3.5. Improved estimates of these parameters were sought using maximum likelihood analysis.

The parameters selected for identification are shown in Table 3.8. These parameters are those judged most important to lateral-directional dynamics. Table 3.9 shows model error covariances and standard deviations before and after the maximum likelihodd identification operation. While the identified parameters do not show large changes in value from the starting values, and none changed sign, the error covariances are reduced for all but the roll rate degree of freedom. Additional analyses are indicated to further reduce the error, beginning with the addition of more variables, particularly C_{n_p}, to the identified set.

NOTES:

1) SEQUENTIAL DOUBLET (δ_e, δ_a, δ_R) MANEUVER
2) NUMBERS ON THE PLOT SHOW THE NUMBER OF DATA POINTS FOR INDICATED α/β REGION

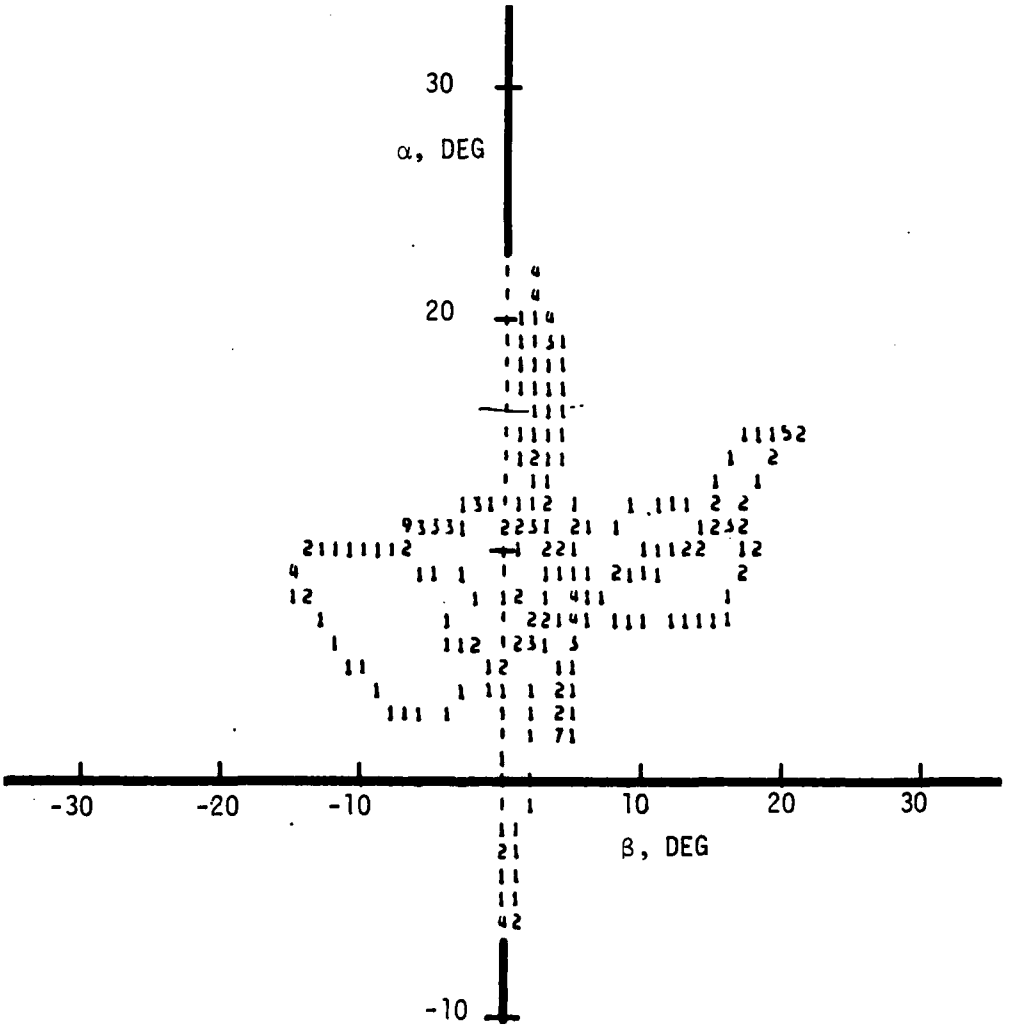

Figure 3.32. α/β Histogram for 2nd Longitudinal Model Prediction Maneuver

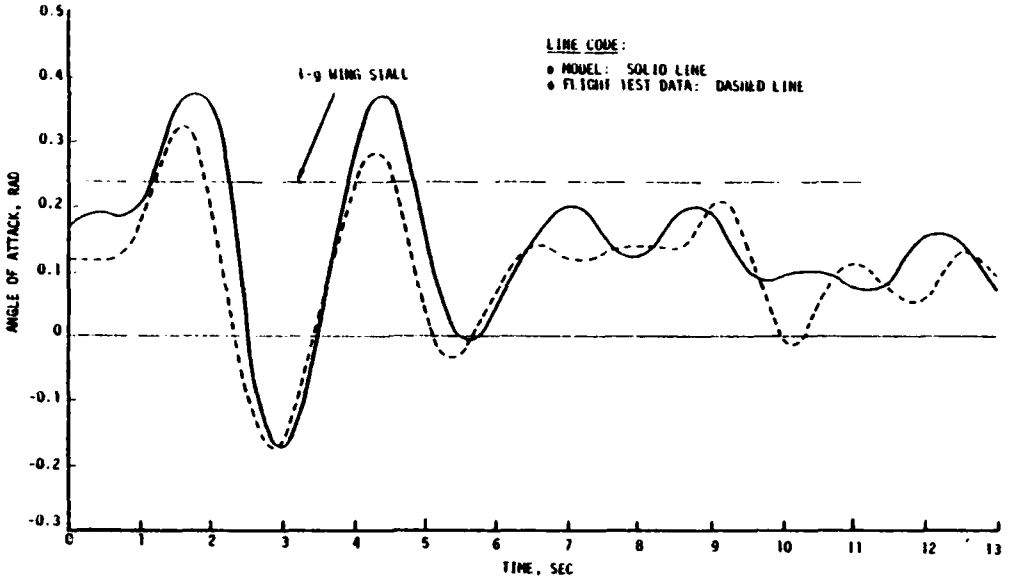

Figure 3.33. Prediction of Sequential Doublet Maneuver with δ_e Random Model: Angle of Attack

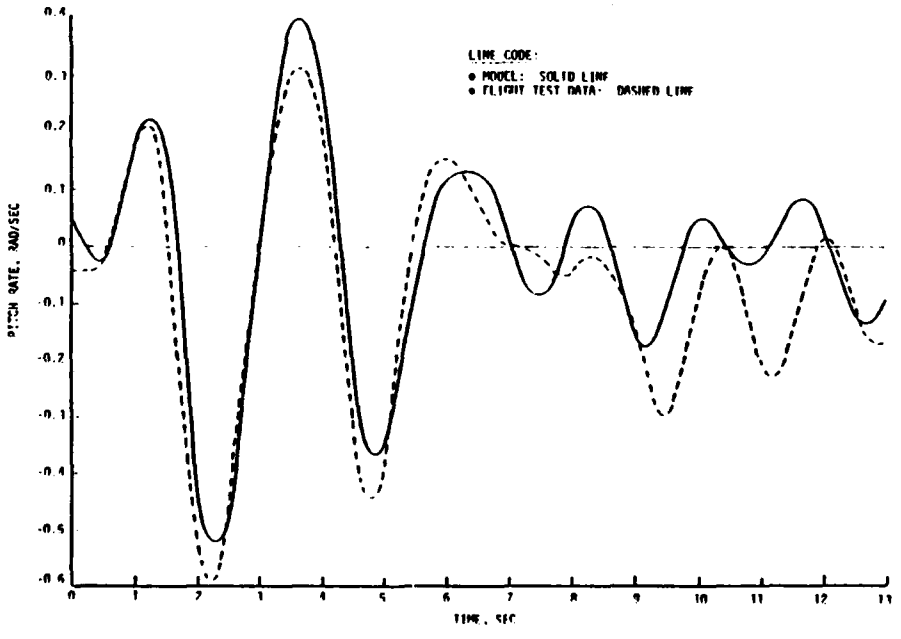

Figure 3.34. Prediction of Sequential Doublet Maneuver with δ_e Random Model: Pitch Rate

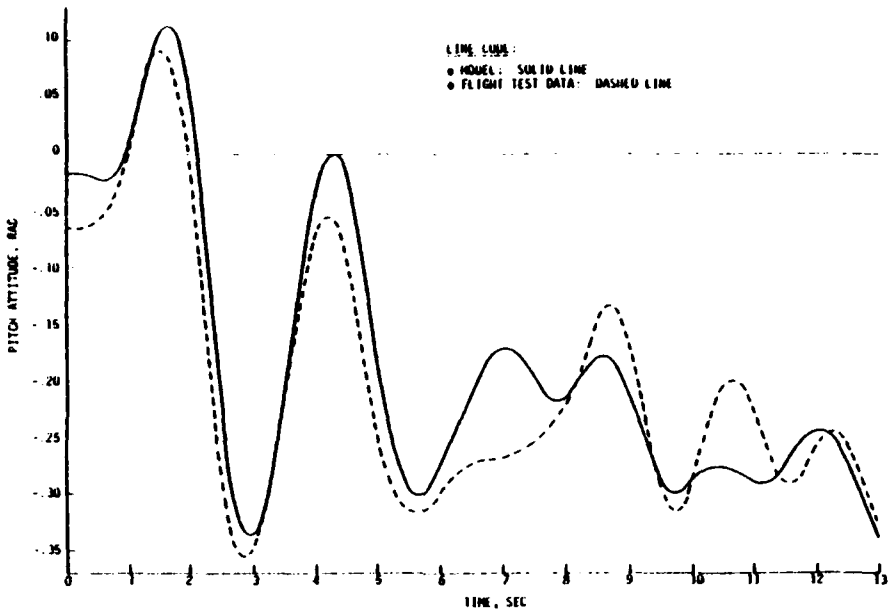

Figure 3.35. Prediction of Sequential Doublet Maneuver with δ_e Random Model: Pitch Attitude

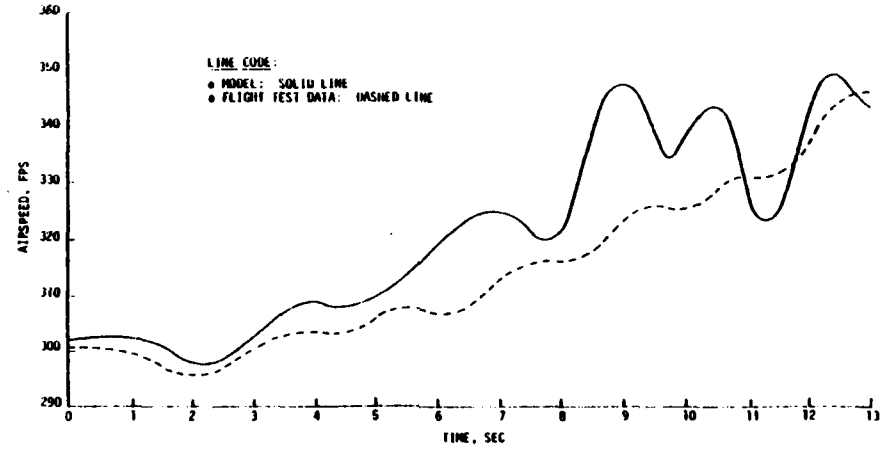

Figure 3.36. Prediction of Sequential Doublet Maneuver with δ_e Random Model: Airspeed

TABLE 3.8. COMPARISON OF STARTING AND IDENTIFIED LATERAL DIRECTIONAL PARAMETERS

PARAMETER*	STARTING	FINAL
C_{ℓ_β}	-.0790	-.0793
C_{ℓ_p}	-.502	-.598
$C_{\ell_{p\alpha}}$	-.690	-.715
$\Delta C_{\ell_p \Delta\alpha l}$	5.85	6.39
C_{ℓ_r}	.292	.268
$C_{\ell_{\delta_a}}$	-.212	-.201
C_{n_β}	.086	.122
$C_{n_{\beta\alpha}}$	-.122	-.112
$C_{n_{\delta_r}}$	-.0526	-.018
C_{Y_β}	-.338	-.334

* Other lateral-directional parameters are as defined in Table 3.5

TABLE 3.9. MEASUREMENT MEAN SQUARE ESTIMATION ERROR: RANDOM AILERON MANEUVER

INITIAL MODEL ERROR COVARIANCE

p	.0354	0	0	0
r	0	.0188	0	0
Φ	0	0	2.854	0
β	0	0	0	.00413

	σ
p	.188 rad/sec
r	.137 rad/sec
ϕ	1.689 rad
β	.064 rad

FINAL MODEL ERROR COVARIANCE

p	.0641	0	0	0
r	0	.00252	0	0
ϕ	0	0	.0490	0
β	0	0	0	.00274

	σ
p	.25 rad/sec
r	.050 rad/sec
ϕ	.221 rad
β	.052 rad

The maneuver selected for analysis here is illustrated by the histogram in Figure 3.37. It represents the response to a random aileron control input at stall. Time history model-measurement comparisons are shown in Figures 3.38 through 3.41, for the variables p, r, ϕ, and β. In general, the agreement is reasonable. Frequencies are well represented, although some underprediction of peak response amplitudes is generally seen. As the model stands, the basic lateral-directional dynamics are well represented.

NOTES:

1) δ_a RANDOM MANEUVER
2) NUMBERS ON THE PLOT SHOW THE NUMBER OF DATA POINTS FOR INDICATED α/β REGION

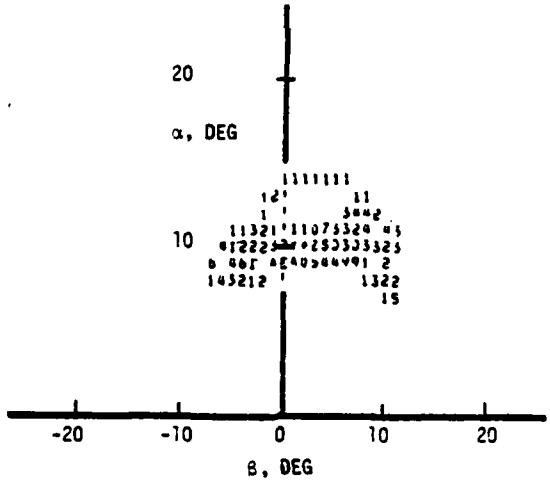

Figure 3.37. α/β Histogram for Lateral/Directional Model Identification

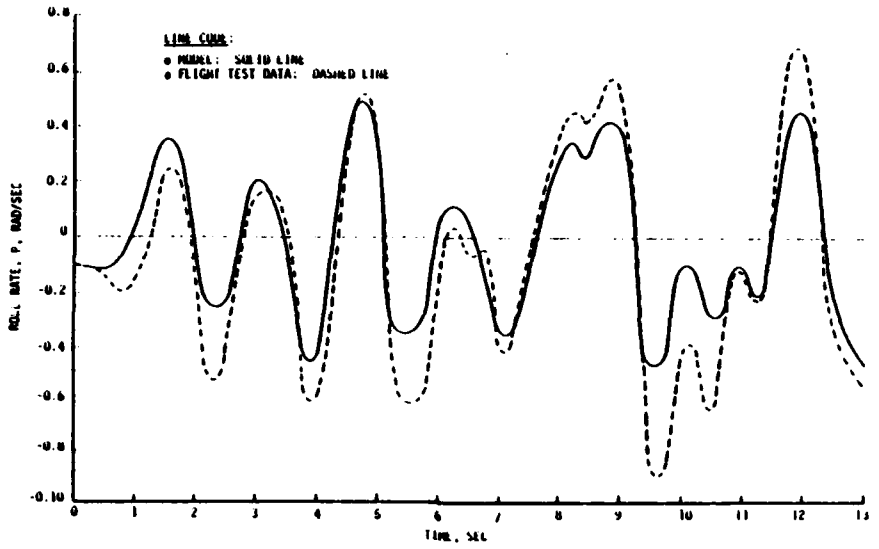

Figure 3.38. Lateral-Directional Model Identification δ_a Random Maneuver: Roll Rate

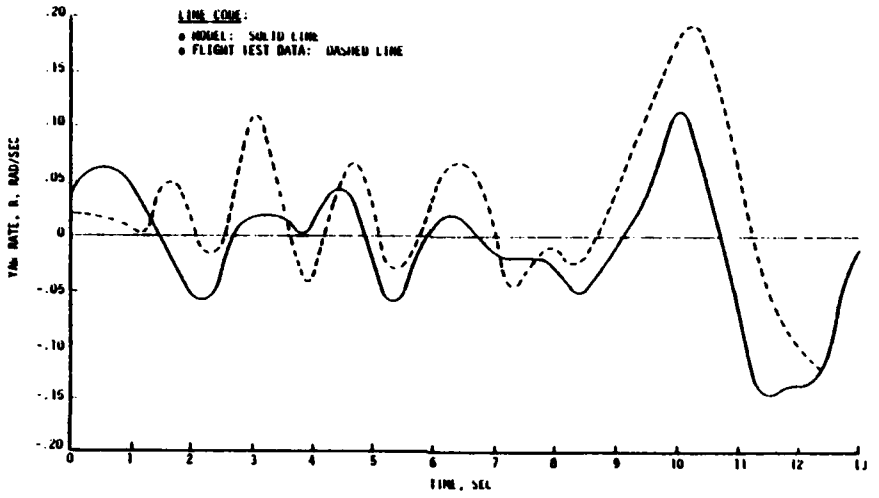

Figure 3.39. Lateral-Directional Model Identification δ_a Random Maneuver: Yaw Rate

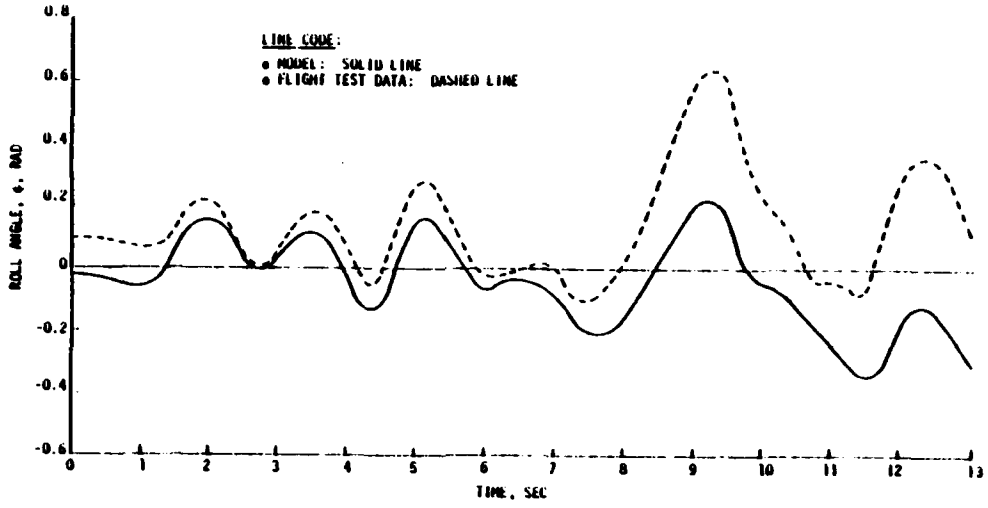

Figure 3.40. Lateral-Directional Model Identification δ_a Random Maneuver: Roll Attitude

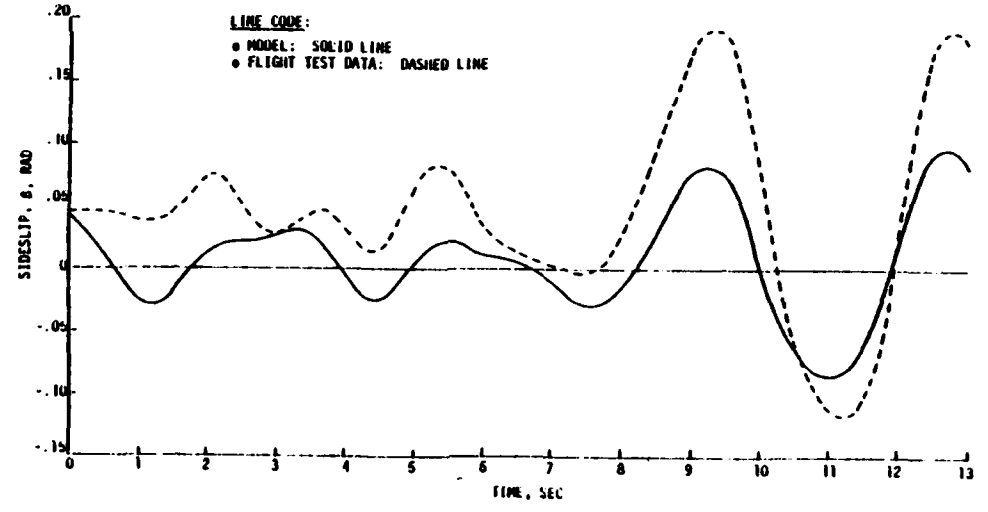

Figure 3.41. Lateral-Directional Model Identification δ_a Random Maneuver: Sideslip

IV. CONCLUSIONS AND RECOMMENDATIONS

4.1 CONCLUSIONS

This study represents one of the first thorough applications of advanced nonlinear system identification techniques to the problem of determining aircraft aerodynamic characteristics in the maximum lift flight regime, and has produced results confirming the capability of these methods to develop realistic and useful dynamics models for flight test data and to provide a valuable guide for data acquisition system specification in future flight test programs. This study also demonstrated the value of employing wind tunnel data and theoretical (or empirical) aerodynamic analyses during the model structure determination stage in order to begin with a basic familiarity with the nature of nonlinearities to be encountered.

The following are the principal conclusions drawn from this work:

(1) Useful and accurate system identification work -- that is, model structure determination and parameter estimation -- can be performed even with poor quality data, due to the ability to reconstruct lost data and filter data with high noise content. Data reconstruction, by computation, differentiation and integration, stands out as an almost indispensable tool for the initial processing of flight data. Examination of the kinematic consistency of the data gives early indication of data acquisition errors.

(2) The most effective approach to model structure determination employs semi-empirical aerodynamic methods (e.g., DATCOM), available wind tunnel data, and aeronautical experience to establish a basic model hypothesis with the minimum number of independent variables and the best estimate of the natures of the nonlinearities expected in the data.

(3) The multiple regression determination of model structures was highly effective in this effort, and identified coefficients of significance with good numerical accuracy, as judged by dynamic simulation results.

(4) Separation of aircraft equations of motion into independent longitudinal and lateral-directional sets and identifying the parameters of each set separately was found to produce good identification of coefficient values while decreasing computational complexity and computer run time.

(5) The generality of the models developed in this study was demonstrated by predicting the time history of one control response maneuver using a model developed from a different maneuver. This generality resulted from the substantial effort taken to define model structures containing aerodynamically relevant nonlinear terms, basing them on the combined results of the analysis of many flight maneuvers and on experience.

(6) The aerodynamic coefficients identified in this effort agreed well in value with wind tunnel data and theoretical aerodynamic calculations of derivatives in the post-stall angle of attack regime. Iterative applications of the model structure determination procedure enabled the optimization of spline function break points to the nonlinearities exhibited by the coefficients within the range of angle of attack covered by the data. Since the majority of the data were in the post-stall regime, identification of coefficients in the low-α, linear regime were expectedly of lower accuracy.

(7) The numerical approach to data processing in this system identification methodology resulted in the identification of such highly nonlinear aerodynamic characteristics as hysteresis in lift, drag and pitching moment around the stall angle of attack, and dynamic deviations with sign changes and reflex curvature versus angle of attack.

(8) The aerodynamic coefficients extracted from the given flight data comprise a basic data set for a flight simulator math model and would be adequate to conduct piloted simulations of vehicle flying qualities in the high angle of attack regime.

The results of this effort are felt to be highly significant in that a unified procedure has been developed which employs all of flight, wind tunnel, and theoretical techniques to achieve improved understanding of aircraft characteristics. The ability to develop accurate models of aircraft behavior from flight measurements presents the opportunity to plan an aircraft program's wind tunnel, theoretical, and flight test work in a coordinated fashion so that each activity fills its role with maximum effectiveness, and the best capabilities of each are used to their full and timely advantage. The success of the system identification procedure demonstrated in this effort signifies that flight data analysis may now be performed in as rigorous and useful a fashion as other experimental and theoretical methods have been used in the past. As a guide to theoretical methods development alone, through its ability to verify predictions of the dynamic stability derivatives of increasing importance in advanced aircraft mission performance, the system identification method can furnish information of value to a wide range of aircraft development programs. And, as future flight test applications extend into the transonic flight regime, the system identification method will, for the first time, enable the study of the complex aerodynamic phenomena that affect aircraft characteristics in that regime and enhance the work that previously could only be done in wind tunnels using extensive subjective engineering judgment. In all, the conclusions reached in this effort are encouraging that an advance in the state of the art of aircraft engineering has been achieved.

4.2 RECOMMENDATIONS

This effort has been a valuable exercise in the identification of nonlinear aerodynamic characteristics, because it has demonstrated the basic viability of the procedure. The following

recommendations refer to improvements which would lead to more effective uses of the system identification procedure and enhanced data processing effectiveness:

(1) Data consistency analysis should be made an integral part of the aircraft parameter identification procedure, to accelerate the process of data reconstruction.

(2) Aircraft instrumentation should be carefully coordinated in terms of redundancy, response, range and resolution to provide optimum data for accurate parameter identification. Careful experimental procedures should be used to assure data acquisition system integrity prior to flight.

(3) Program development efforts should be directed toward automating the powerful spline-function representation of coefficients within the regression program used in model structure determination, as the existence of an accurate model greatly improves the accuracy of later parameter identification results.

(4) Further work should be directed toward developing a general nonlinear aerodynamic identification model suitable for fixed-wing aircraft analysis. Following the approach taken in this effort, the model should be in a form readily implementable in a flight simulator math model.

(5) Subsequent efforts should be directed toward the integration of system identification (as applied to flight test), wind tunnel experimentation, and theoretical methods into procedures and tools by which they may most effectively contribute to the needs of aircraft development and evaluation programs. Commonalities in requirements and capabilities, and areas in which strengths can be combined, should be determined. A research program in this area is almost certain to produce interesting and useful results leading toward a unified aerodynamic treatment of aircraft.

(6) Extensions of this method to the determination of structural parameters from flight test data, and the study of their correlation to aerodynamic results, particularly in the transonic regime, should be pursued.

These recommendations, it is felt, will eanble the results of this study to be fully utilized in improving the ultimate effectiveness of aircraft engineering activities.

REFERENCES

1. Hall Jr., W.E., "Identification of Aircraft Stability and Control Derivatives for the High-Angle-of-Attack Regime," Tech. Rept. No. 1, prepared for the Office of Naval Research under Contract N00014-72-C-0328, June 1973.

2. Hall Jr., W.E., Gupta, N.K., and Smith, R.G., "Identification of Aircraft Stability and Control Derivatives for the High-Angle-of-Attack Regime," Tech. Rept. No. 2, prepared for the Office of Naval Research under Contract N00014-72-C-0328, 1974.

3. Gupta, N.K. and Hall Jr., W.E., "Input Design for Identification of Aircraft Stability and Control Coefficients," NASA CR-2493, Feb. 1975.

4. Mehra, R.K. and Gupta, N.K., "Status of Input Design for Aircraft Parameter Identification," presented at AGARD Specialist's Conference on Methods for Aircraft State and Parameter Estimation, NASA Langley Research Center, Hampton, VA, Nov. 1974.

5. Gupta, N.K. and Hall Jr., W.E., "SCIDNT $\pm$ Theory and Applications," Tech. Rept. No. 3, prepared for the Office of Naval Research and Naval Air Test Center, Contract No. N00014-72-C-0328, Dec 1974.

6. Burton, R.A., Latham, L.J., "Verification of S-3A Lateral-Directional Power Approach Characteristics using a Maximum Likelihood Parameter Identification Technique," Report No. SA-27R-76, Naval Air Test Center, 28 May 1976.

7. Burton, R.A., and Bischoff, D.E., "More Effective Aircraft Stability and Control Testing through Use of System Identification in Technology," TM76-25A, Naval Air Test Center, 4 Nov. 1976.

8. Gupta, N.K. and Hall, Jr., W.E., "Methods for the Real-Time Identification of Vehicle Parameters," Tech. Rept. No. 4, prepared for the Office of Naval Research under Contract N00014-72-C-0328, Feb. 1975.

9. Scheutz, A.J. and Bailey, D.B., "Low Speed Wind Tunnel Investigation of a .09 Scale Naval Model T-2C Subsonic Jet Trainer Aircraft, From -8 to +83 Degrees Angle of Attack," Report No. NADC-73259-30, Dec. 1973.

10. Barnhart, B., "Estimated Dynamic Derivatives for T-2C Aircraft from -8 to +45 Degrees Angle of Attack," Tech. Memo Rept. No. BAR2-76, Vol. II, Nov. 1976.

11. Hall Jr., W.E. and Gupta, N.K., "System Identification for Nonlinear Aerodynamic Flight Regimes," Journal of Space Craft and Rockets, Vol. 14, No. 2, Feb 1977, pp. 73-80.

12. Gupta, N.K. and Hall Jr., W.E., "Identification of T-2 Aerodynamic Derivatives from Flight Data," Final Report on Contract N62269-72-0597, March 1975.

APPENDIX A
T-2C SPECIFICATIONS

WING

S_W	Total area (includes flap, aileron and 39.39 ft^2 covered by fuselage)	254.86 ft^2
A_W	Net surface area (wetted)	424.85 ft^2
b_W	Span (perpendicular to plane of symmetry) including tiptanks	38.13 ft
AR_W	Aspect Ratio	5.07
λ_W	Taper Ratio	.496
Γ_W	Dihedral Angle	+3°
	Chord (in streamline direction)	
c_r	Root (Wing Sta. 0)	114.20 in
c_t	Tip Chord (Wing Sta. 214.242)	56.63 in
	(Equivalent)	
$\bar{c}_W$	Mean aerodynamic chord	88.88 in
	(Wing Sta. 95.078)	
	Location of 25% MAC	F.S. 219.697
Λ_W	Sweepback of 25% element	2°17'
i_W	Incidence angle	
	Root Chord	2°
	Tip Chord	-1°
	Airfoil Section (root and tip in streamline direction)	$NASA64_1A212$ 2 = .8* (MOD) (flaps and ailerons rigged 3° up)
	*NAA Modified	
Ω_W	Rate of Taper	0.2671

FLAP (Data for One)

	Type	Single Slotted
S_f	Area	22.78 ft^2
b_f	Span (perpendicular to plane of symmetry)	101.75 in
c_i	Inboard chord (Wing Sta. 27.09)	39.39 in
c_o	Outboard chord (Wing Sta. 127.54)	29.63 in
c_f/c_w	Ratio flap chord to wing chord (avg.)	.37
$b_f/\frac{b_w}{2}$	Ratio flap span to wing semi-span	.475
δ_f	Flap deflection, maximum (from uprigged position)	33°
	Flap in neutral position	3° Up

AILERON

	Type	Straight Sided
S_a	Area (aft of hinge line and including tab)	9.5 ft^2
b_a	Span (perpendicular to plane of symmetry)	79.57 in
c_i	Inboard chord (Wing Sta. 128.69)	20 in
c_o	Outboard chord (Wing Sta. 208.26)	14.66 in
c_a/c_w	Ratio aileron chord (aft H.L.) to wind chord	.25
$b_a/\frac{b_w}{2}$	Ratio aileron span to wind semi-span	.374
δ_a	Aileron deflection, maximum (from neutral position)	-12° Up, +13° Dn
	Aileron in neutral position	3° Up
	Aerodynamic Balance	Sealed paddle balance
S_b	Balance area forward of the H.L. (including 50% of fabric seal)	4.45 ft^2
c_b/c_a	Ratio balance chord to aileron chord	.42

AILERON - (Cont'd)

	Static balance	Weighted paddle balance
	Irreversible full power system	Hydraulic

AILERON TRIM TAB

	Ground adjustable fixed tab on each aileron	
S_a	Area (each)	.07 ft^2

HORIZONTAL TAIL*

S_h	Total area (includes 3.07 ft^2 covered by vertical tail and fairing)	72.29 ft^2
S_{net_h}	Net area	69.22 ft^2
A_h	Net surface area (wetted)	146.38 ft^2
b_h	Span	17.91 ft
AR_h	Aspect Ratio	4.42
λ_h	Taper Ratio	0.50
Γ_h	Dihedral Angle	0°
Λ_h	Sweepback of 25% element	15°
	Chord (in streamline direction)	
c_r	Root (H.T. Sta. 0)	64.61 in
c_t	Equivalent tip chord (H.T. Sta. 106.488)	33.05 in
$\bar{c}_h$	Mean aerodynamic chord (H.T. Sta. 47.78)	50.447 in
i_h	Incidence angle	0°
	Airfoil section (root and tip in streamline direction)	NASA 65A012

*Percent lines base on horizontal prior to addition of trailing edge extension.

HORIZONTAL TAIL - (Cont'd)

l_h	Tail length (.25 $\bar{c}_w$ to .25 $\bar{c}_h$)	202.58 in

HORIZONTAL STABILIZER

S_s	Area stabilizer, total	42.5 ft^2
i_s	Stabilizer incidence angle	0°

ELEVATOR

S_e	Total area (excluding balance area forward of the hinge line)	21.00 ft^2
b_e	Span (between equivalent chords) (one elevator only)	101.97 in
c_i	Inboard chord (B.P. 3.906)	18.85 in
c_o	Outboard chord (B.P. 105.877)	10.52 in
c_e/c_h	Ratio elevator chord (aft H.L.) to horizontal tail chord	.310
b_e/b_h	Ratio elevator span to horizontal tail span	0.936
δ_e	Elevator deflection maximum	27° Up, 15° Dn
	Boost: Push force 2.95:1	Hydraulic
	Pull force 2.95:1 to 8 lbs	
	then 6.0:1	
	Static balance	Weighted Leading Edge
	Aerodynamic balance	Overhang
S_b	Balance area forward of hinge line	5.72 ft^2
c_b/c_e	Ratio balance chord to elevator chord	0.322
	Nose factor	0.60
	Point of tangency for nose factor is at elevator hinge line	

ELEVATOR TRIM TAB

S_t	Area (each)	2.36 ft^2
b_t	Span, Equivalent (B.P. 8.93 to 54.53)	46.10 in
c_t	Chord, constant	6.5 in
b_t/b_e	Ratio tab span to elevator span	0.462 in
δ_t	Tab deflection	L.H. 10° Up, 13° Dn R.H. 0° Up, 13° Dn

VERTICAL TAIL

S_v	Total area (includes 4.38 ft^2 blanketed by fuselage plus 2.14 ft^2 blanketed by horizontal tail)	40.33 ft^2
S_{net_v}	Net area	33.86 ft^2
A_v	Net surface area (wetted)	79.18 ft^2
A_d	Net surface area of dorsal fin (wetted)	18.12 ft^2
b_v	Span, unblanketed	8.04 ft
AR_v	Aspect Ratio	1.80
λ_v	Taper Ratio	.375
c_r	Chord (in streamline direction)	
	Root (W.P. + 33.000)	78.14 in
c_t	Equivalent Tip Chord (W.P. + 129.41)	29.38 in
$\bar{c}_v$	Mean aerodynamic chord (W.P. + 73.92)	58.47 in
Λ_v	Sweepback (25% chord)	30°
	Airfoil Section	NASA 63A012
l_v	Tail length (.25 $\bar{c}_w$ to .25 $\bar{c}_v$)	194.05 in

VERTICAL FIN

S_f	Area (including 2.14 ft^2 blanketed by horizontal tail and excluding dorsal fin)	29.87

VERTICAL FIN (Cont'd)

i_f	Angle with respect to airplane plane of symmetry	0°
RUDDER		
S_r	Total area	9.13 ft^2
	S_{r_u} Upper surface	3.23 ft^2
	S_{r_l} Lower surface	5.90 ft^2
b_r	Span, equivalent	
	b_{r_u} Upper surface	31.94 in
	b_{r_l} Lower surface	42.99
c_{r_u}	Upper chord (W.P. 96.00)	12.59 in
c_{r_l}	Lower chord (W.P. + 9.91)	22.45 in
c_r/c_v	Ratio rudder chord (aft H.L.) to vertical tail chord	
	c_r/c_v Upper surface @ W.P. 96.00	.266
	c_r/c_v Lower surface	.250
δ_r	Rudder deflection, maximum	25° Rt., 25° Lt.
	Boost	None
	Aerodynamic balance	Overhang
S_b	Balance area forward of hinge line	2.41 ft^2
c_b/c_r	Ratio balance chord to rudder chord	
	c_b/c_{r_u} Upper surface @ W.P. 96.00	.234
	c_b/c_r Lower surface	.24
	Static balance	Weighted leading edge
	Nose factor	0.40
	Point of tangency for nose factor is at rudder hinge line	

RUDDER TRIM TAB		
S_t	Area	1.60 ft^2
b_t	Span, equivalent (W.P. 14.94 to W.P. 53.00)	38.06 in
c_t	Chord, constant	6.0 in
b_t/b_r	Ratio tab span to rudder span	.508
δ_t	Tab deflection, maximum	7° Rt., 7° Lt.
FUSELAGE		
l_f	Length (actual)	34.58 ft
F_f	Maximum frontal area (basic fuselage)	15.75 ft^2
w_f	Maximum width (basic fuselage) F.S. 169	54 in
h_f	Maximum depth	
	Basic fuselage over canopy (F.S. 169)	88.1 in
	Including ducts (F.S. 214)	73.9 in
A_f	Net surface area	221.11 ft^2
L/D	Fineness ratio (actual)	5.91
CANOPY		
l_c	Length (actual)	19.75 ft
F_c	Maximum frontal area	3.70 ft^2
A_c	Net surface area	73.10 ft^2
L/D_c	Fineness ratio (actual)	8.8
NACELLE		
l_n	Length (actual)	23.71 ft
F_n	Maximum frontal area	10.50 ft^2
A_n	Net surface area	206.0 ft^2
	Inlet area (includes gutters)	3.1 ft^2
L/D_n	Fineness ratio (actual)	5.025

SPEED BRAKE (Data for one side only)

	Type	One Piece
	Location	Side of Aft Fuselage
	Number	Two
S_j	Area (Planform)	8.00 ft^2
F_j	Area (frontal)	4.24 ft^2
δ_j	Maximum deflection	32°

TIP TANK (Data for one tank only)

l_{tt}	Overall length	142.75 in
d_{tt}	Maximum diameter (Tank Sta. 61.875)	20.00 in
L/D	Fineness ratio	7.14
Ss_{tt}	Side area (projected)	14.1 ft^2
Sp_{tt}	Planform area (projected)	14.2 ft^2
	Volume	15.3 ft^3
A_{tt}	Total Surface Area	44.30 ft^2
$A_{net_{tt}}$	Net Surface Area (wetted)	42.40 ft^2